Title

The Influenza A Virus Endoribonuclease PA-X Usurps Host mRNA Processing Machinery to Limit Host Gene Expression

Journal

Cell Reports, 27(3)

ISSN

2639-1856

Authors

Gaucherand, Lea

Porter, Brittany K

Levene, Rachel E

et al.

Publication Date

2019-04-01

DOI

10.1016/j.celrep.2019.03.063

Peer reviewed

HHS Public Access

Author manuscript

Cell Rep. Author manuscript; available in PMC 2019 May 03.

Published in final edited form as:

Cell Rep. 2019 April 16; 27(3): 776–792.e7. doi:10.1016/j.celrep.2019.03.063.

The Influenza A Virus Endoribonuclease PA-X Usurps Host mRNA Processing Machinery to Limit Host Gene Expression

Lea Gaucherand[1,2,6], **Brittany K. Porter**[3,6], **Rachel E. Levene**[1,2], **Emma L. Price**[3], **Summer K. Schmaling**[2], **Chris H. Rycroft**[4,5], **Yuzo Kevorkian**[1,2], **Craig McCormick**[3,*], **Denys A. Khaperskyy**[3,*], and **Marta M. Gaglia**[1,2,7,*]

[1]Graduate Program in Molecular Microbiology, Sackler School of Graduate Biomedical Sciences, Tufts University, Boston, MA, USA

[2]Department of Molecular Biology and Microbiology, Tufts University School of Medicine, Boston, MA, USA

[3]Department of Microbiology & Immunology, Dalhousie University, Halifax, NS, Canada

[4]Paulson School of Engineering and Applied Sciences, Harvard University, Cambridge, MA, USA

[5]Computational Research Division, Lawrence Berkeley National Laboratory, Berkeley, CA, USA

[6]These authors contributed equally

[7]Lead Contact

SUMMARY

Many viruses shut off host gene expression to inhibit antiviral responses. Viral proteins and host proteins required for viral replication are typically spared in this process, but the mechanisms of target selectivity during host shutoff remain poorly understood. Using transcriptome-wide and targeted reporter experiments, we demonstrate that the influenza A virus endoribonuclease PA-X usurps RNA splicing to selectively target host RNAs for destruction. Proximity-labeling proteomics reveals that PA-X interacts with cellular RNA processing proteins, some of which are partially required for host shutoff. Thus, PA-X taps into host nuclear pre-mRNA processing mechanisms to destroy nascent mRNAs shortly after their synthesis. This mechanism sets PA-X apart from other viral host shutoff proteins that target actively translating mRNAs in the cytoplasm. Our study reveals a unique mechanism of host shutoff that helps us understand how influenza viruses suppress host gene expression.

*Correspondence: craig.mccormick@dal.ca (C.M.), d.khaperskyy@dal.ca (D.A.K.), marta.gaglia@tufts.edu (M.M.G.).

AUTHOR CONTRIBUTIONS

Conceptualization, C.M., D.A.K., M.M.G.; Investigation, L.G., B.K.P., R.E.L., E.L.P., S.K.S, Y.K., D.A.K., and M.M.G.; Formal Analysis, C.H.R. and M.M.G.; Writing, L.G., R.E.L., C.M., D.A.K., and M.M.G.; Funding Acquisition, C.M. and M.M.G.

SUPPLEMENTAL INFORMATION

Supplemental Information can be found online at https://doi.org/10.1016/j.celrep.2019.03.063.

DECLARATION OF INTERESTS

The authors declare no competing interests.

SUPPORTING CITATIONS

The following references appear in the Supplemental Information: Abernathy et al. (2015); Ank et al. (2006); Arias et al. (2014); Feng et al. (2013); Hu et al. (2013); Morgano et al. (2012); Wang et al. (2012).

In Brief

Gaucherand et al. uncover a unique relationship between RNA degradation by the influenza A virus ribonuclease PA-X and host RNA splicing, which allows PA-X to selectively target host RNAs for destruction.

Graphical Abstract

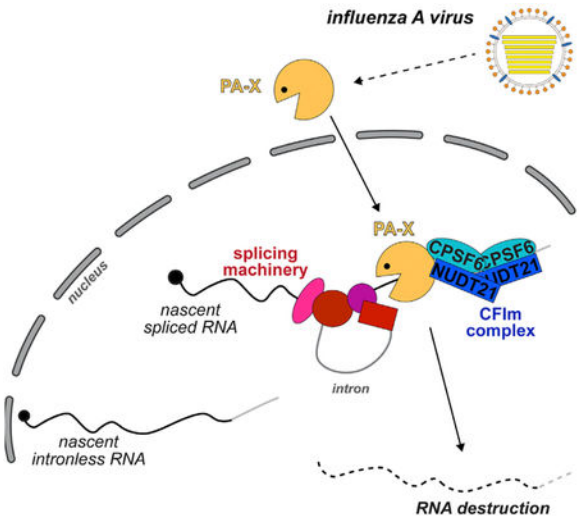

INTRODUCTION

Despite their small genomes, influenza A viruses (IAVs) dedicate multiple proteins to the suppression of host gene expression, or “host shutoff,” which limits host antiviral responses. One of these IAV host shutoff proteins is the endoribonuclease PA-X, which selectively degrades host RNAs (Jagger et al., 2012; Khaperskyy et al., 2016) and limits innate immune responses *in vivo*. PA-X-deficient viruses induce stronger innate immune and inflammatory responses in mice, chickens, and pigs (Gao et al., 2015; Gong et al., 2017; Hayashi et al., 2015; Hu et al., 2015, 2016; Jagger et al., 2012; Xu et al., 2017). In some IAV strains, the immune-evasion activity of PA-X reduces inflammation-induced pathology, thereby protecting the host and reducing mortality (Gao et al., 2015; Gong et al., 2017; Hu et al., 2015, 2016; Jagger et al., 2012). While the role of PA-X in immune evasion is well established, its molecular mechanism of action remains poorly understood.

PA-X is produced by ribosomal frameshifting during the translation of the polymerase acidic protein (PA) mRNA (Firth et al., 2012; Jagger et al., 2012). The frameshift generates a protein with the PA amino-terminal ribonuclease (RNase) domain fused to a unique carboxy-terminal domain known as the X-open reading frame (X-ORF). The X-ORF is required for PA-X function (Hayashi et al., 2016; Khaperskyy et al., 2016; Oishi et al., 2015). Despite this non-canonical production mechanism, PA-X is en-coded by all IAV strains (Shi et al., 2012). We previously reported that PA-X selectively degrades RNAs transcribed by host RNA polymerase II (Pol II), but not other polymerases (Khaperskyy et al., 2016). This characteristic leads to the protection of viral RNAs created by the viral

RNA-dependent RNA polymerase (RdRp) (Khaperskyy et al., 2016). However, the mechanism for PA-X targeting of Pol II transcripts is not known.

Other viruses encode host shutoff RNases that selectively target Pol II transcripts, including alphaherpesviral vhs proteins, gammaherpesviral SOX/BGLF5 proteins, and the severe acute respiratory syndrome-related coronavirus (SARS-CoV) non-structural protein 1 (nsp1) (Covarrubias et al., 2009, 2011; Elgadi et al., 1999; Gaglia et al., 2012; Glaunsinger and Ganem, 2004a; Kamitani et al., 2006; Rowe et al., 2007). However, SARS nsp1 and the herpesviral host shutoff proteins operate in the cytoplasm and only degrade transcripts that are bound by components of the protein synthesis machinery (Covarrubias et al., 2011; Doepker et al., 2004; Feng et al., 2001, 2005; Gaglia et al., 2012; Kamitani et al., 2009). By contrast, PA-X accumulates in the nucleus, and the protein synthesis machinery has no role in RNA targeting and degradation (Hayashi et al., 2016; Khaperskyy et al., 2016). Our previous analysis of select transcripts suggests that not all Pol II transcripts are equally susceptible to PA-X degradation (Khaperskyy et al., 2016), similar to reports for other viral host shutoff RNases (Esclatine et al., 2004; Glaunsinger and Ganem, 2004b). In agreement with this, a recent study of the host transcriptome in IAV-infected cells showed that certain functional classes of RNAs were spared from shutoff, although no specific link to PA-X activity was established (Bercovich-Kinori et al., 2016). By contrast, in the context of studying the relative contribution of IAV PA-X and NS1 proteins to host shutoff, Toru Takimoto's group recently reported that host mRNAs targeted by PA-X do not clearly belong to specific functional classes, whereas there is functional specificity among NS1 targets (Chaimayo et al., 2018). These findings suggest that PA-X may have a unique mechanism to selectively target host RNAs in the nucleus, perhaps in conjunction with RNA processing and the assembly of functional messenger ribonucleoprotein (mRNP) complexes.

Here, we report transcriptome-wide analysis of PA-X targets in human lung A549 cells, in both *de novo* infection and ectopic expression models. This analysis revealed that PA-X susceptibility is tightly linked to Pol II transcript splicing. Moreover, we identified host proteins involved in mRNA processing that associate with the C-terminal X-ORF, suggesting that PA-X target selection may involve physical interactions with components of the host mRNA processing machinery.

RESULTS

PA-X Causes Global Changes in RNA Levels during Infection

To determine the scope of PA-X specificity for host Pol II transcripts, we profiled RNA levels in cells infected with wild-type (WT) and PA-X-deficient IAVs. To generate PA-X-deficient mutants in the well-characterized strain A/PuertoRico/8/1934 H1N1 (PR8), we introduced 2 mutations in the frameshifting site and a nonsense mutation in PA-X, L201Stop, that truncated the X-ORF after 9 amino acids (aa); we called this virus PA(ΔX) (Figure 1A). These mutations were designed to be silent in the PA ORF. We previously used a strain with only the frameshifting mutations, IAV PA(fs) (Figure S1A) (Khaperskyy et al., 2016), but we created IAV PA(ΔX) to ensure that any residual frameshifting would produce a non-functional PA-X. We confirmed that the 9-aa truncated PR8 PA-X was largely inactive, as it lost the ability to degrade a β-globin reporter, whereas an X-ORF truncation to

15 aa retained activity (Figure 1B). The β-globin reporter includes the two introns of the native β-globin gene, and expresses an mRNA that is spliced. The results in Figure 1B recapitulate previous findings using truncations in PA-X variants from other strains (Hayashi et al., 2016; Oishi et al., 2015). We also generated a virus with only the L201Stop mutation and called it "X9" (Figure S1A). We chose to use the PR8 strain because it lacks two other known IAV host shutoff mechanisms; its NS1 protein does not block host mRNA processing (Das et al., 2008; Salvatore et al., 2002), and its RdRp does not trigger Pol II degradation (Rodriguez et al., 2009).

Using high-throughput RNA sequencing (RNA-seq), we found that the infection of cells with WT IAV caused a dramatic global decrease in transcript levels compared to mock-infected cells (Figure 1C; Data S1). However, a small fraction of transcripts escaped shutoff (right tail end of distribution; Figure 1C). By contrast, shutoff was substantially attenuated in IAV PA(ΔX)-infected cells. Cells infected with strains carrying either the PA(X9) or PA(fs) mutations also displayed attenuated host shutoff, and the defect was similar in all three mutants (Figure S1B). This demonstrates that X-ORF truncation disrupts PA-X function during infection, as predicted from ectopic PA-X expression studies (Hayashi et al., 2016; Khaperskyy et al., 2016; Oishi et al., 2015). Infection rates by WT and mutant viruses were comparable, based on immunofluorescence staining and viral protein levels (Figures S2A and S2B). We also measured the nuclear accumulation of cytoplasmic poly(A) binding protein (PABP), a well-described consequence of host shutoff (Khaperskyy et al., 2014; Kumar and Glaunsinger, 2010; Kumar et al., 2011; Lee and Glaunsinger, 2009). Infection with PA(X9) and PA(ΔX) viruses resulted in significantly lower rates of PABP nuclear accumulation compared to WT, confirming the impairment of host shutoff (Figures S2A and S2C). Lastly, our RNA-seq results strongly correlated with those from a previous transcriptome profile of IAV PR8-infected cells (Bercovich-Kinori et al., 2016), despite the differences in multiplicity of infection (MOI) and time course of analysis (Figure 1D). These data demonstrate that PA-X controls the levels of the majority of host RNAs during infection.

PA-X Causes Global Downregulation of Host RNAs in an Ectopic Expression Model

To simplify our system, we also examined changes in RNA levels after ectopic PA-X expression. We used a doxycycline-inducible PA-X expression system, "iPA-X" cells (Khaperskyy et al., 2016), to induce the expression of WT PA-X or the catalytically inactive D108A mutant in A549 cells. Because iPA-X cells were clonally selected, we analyzed 2 independently generated cell lines for each variant. As expected from previous results with targeted RT-qPCR and metabolic labeling (Hayashi et al., 2015; Jagger et al., 2012; Khaperskyy et al., 2016), WT PA-X robustly downregulated steady-state transcript levels (Figure 2A; Data S2). The degree of host shutoff correlated with the levels of PA-X (percentage of total reads mapping to PA-X: WT #1 = 0.005%–0.006%, WT #10 = 0.023%–0.026%) and was dependent on RNase activity, because expression of the PA-X catalytic mutant had no effect (Figure 2A). A substantial minority of transcripts was unaffected by PA-X expression (right tail end of distributions; Figure 2A). Furthermore, we observed a highly significant correlation between the PA-X-dependent downregulation of RNAs in the ectopic PA-X expression system and in virus-infected cells (Figure 2B). This indicates that

PA-X largely targets the same RNAs in the absence of other viral proteins and that the ectopic expression model accurately reflects the contribution of PA-X to host shutoff during infection. To further validate these findings, we selected representative RNAs, choosing RNAs that were strongly downregulated (glyceraldehyde-3-phosphate dehydrogenase [GAPDH], glucose-6-phosphate dehydrogenase [G6PD]) or largely unaffected (heterogeneous nuclear ribonucleoprotein A0 [HNRNPA0], TATA-box binding protein associated factor 7 [TAF7], enhancer of polycomb homolog 1 [EPC1]) in both *de novo* infection and ectopic expression models. We then validated the change in RNA levels in iPA-X cells by RT-qPCR. The RT-qPCR results agreed with the RNA-seq data in terms of the selective effects on the tested transcripts (Figure 2C). By contrast, doxycyline-inducible expression of the catalytically inactive PR8 PA-X D108A mutant or the PA-X RNase domain (aa 1–191, "N term") did not affect the level of any of the tested transcripts (Figure 2C). Expression of PA-X or the RNase domain was confirmed by western blotting (Figure 2D). Because the RNase domain alone is active *in vitro* (Bavagnoli et al., 2015; Dias et al., 2009; Yuan et al., 2009), this result confirms that it is specifically the activity of PA-X and not the overexpression of any active RNase that controls RNA levels in the iPA-X cells. Moreover, the mRNA levels were similarly affected by the expression of PA-X from the A/Udorn/72 H3N2 (Udorn) strain, suggesting that target selection by PA-X is conserved among virus strains (Figure 2C). These data demonstrate that PA-X broadly targets RNA for degradation, while a subset of RNAs remains unaffected.

Specific Functional Classes of Host RNAs Are Differentially Sensitive to PA-X

Although most RNAs were downregulated by PA-X, the levels of ~25% of RNAs remained largely unchanged (Figures 1C and 2A). To identify resistant RNAs, we used *k*-means clustering to group RNAs with similar patterns of regulation (Gasch and Eisen, 2002). Clustering was carried out based on the relative RNA levels in PA-X-overexpressing (OE) cells versus control cells or IAV-versus mock-infected cells in our 8 datasets (Figures 1C, 2A, and S1B). Two sets of RNAs making up 55% of the RNAs that were detected in all conditions were identified as true PA-X targets (Figure 3A; Data S1a and S2a). These RNAs were downregulated in a PA-X-dependent manner both during infection and by PA-X ectopic expression. The RNAs in the first set were completely PA-X-specific, as their levels were largely unchanged in IAV PA(ΔX)-infected cells (Figure 3A, left). The RNAs in the second set were PA-X sensitive, but were partially downregulated by other mechanisms during IAV PA(ΔX) infection (Figure 3A, right). By contrast, 28% of the RNAs were PA-X resistant and were not downregulated by infection or PA-X expression (Figure 3B; Data S1b and S2b). In addition, the *k*-means algorithm identified a group of RNAs that were downregulated during infection by a PA-X-independent mechanism and yet were PA-X sensitive in PA-X-expressing cells (Figure 3C; Data S1c and S2c). The levels of these transcripts may be substantially decreased by other regulatory mechanisms during infection, such that their targeting by PA-X is masked. Based on Gene Ontology (GO) term analysis, the host shutoff-resistant RNAs were significantly enriched for genes involved in transcription and translation, including ribosomal RNA processing, ribosomal proteins, and membrane protein synthesis (Figure 3D). This result is consistent with the IAV requirement for host biosynthetic machinery and observations by Bercovich-Kinori et al. (2016). These

results suggest that while PA-X can target many RNAs, it retains some specificity for functional classes of RNAs.

In addition to this unbiased analysis, we examined how PA-X expression affected the levels of interferon-stimulated genes (ISGs), which are induced in infected cells and function in antiviral defense (Schoggins et al., 2011). We observed that although ISGs were induced during IAV infection, as shown by their higher expression compared to all of the detected RNAs, their levels were even higher in the absence of PA-X (Figure 3E). While the activity of PA-X is clearly not limited to ISGs, these data indicate that PA-X can contribute to dampening the cell-intrinsic response to infection.

PA-X Strongly and Preferentially Downregulates Spliced Pol II Transcripts

We previously showed that PA-X selectively degrades RNA transcribed by Pol II and spares Pol I and Pol III transcripts (Khaperskyy et al., 2016). Although all cellular transcripts are modified post-synthesis, only Pol II transcripts can be spliced. The process of RNA splicing is mechanistically linked to transcription, as recruitment of the spliceosome is mediated by the C-terminal domain of the large subunit of Pol II (Gu et al., 2013). However, a subset of Pol II transcripts naturally lacks introns. When we analyzed spliced versus intronless RNAs separately, we found that PA-X downregulated spliced RNAs more than intronless RNAs (Figure 4A). Our targeted validation also showed that two intronless mRNAs, TAF7 and HNRNPA0, were not downregulated by PA-X (Figure 2C), and, as mentioned above, the β-globin reporter used in Figure 1B encodes a spliced mRNA. Moreover, during infection, the downregulation of spliced RNAs was clearly dependent on PA-X, whereas most of the downregulation of intronless RNAs was PA-X independent (Figure 4B). For these analyses, we only included intronless RNAs longer than 300 nt, excluding small non-coding RNAs and ensuring that the length distribution was similar between spliced and intronless RNAs. We also analyzed how the number of exons affected RNA downregulation, as the number of splice sites varies dramatically among spliced RNAs. There was a significant negative correlation between the number of exons in a transcript and its steady-state levels in PA-X-expressing and infected cells (PA-X-expressing cells: Spearman's $\rho = -0.52$, Figure 4C; IAV-infected cells: Spearman's $\rho = -0.47$, Figure S3A). This result suggests that RNAs with more exons are more susceptible to PA-X degradation. However, the number of exons in an RNA is often proportional to RNA length. A prior study reported a relation between IAV host shutoff and transcript length (Bercovich-Kinori et al., 2016). Likewise, there was a correlation between degradation and RNA length in our data (Spearman's $\rho = -0.38$ for both PA-X-expressing [Figure 4D] and IAV-infected cells [Figure S3B]). To determine whether exon number or transcript length was important, we examined RNAs of similar length or with a specific number of exons. We still found a robust negative correlation between relative RNA levels in the presence of PA-X and exon number among RNAs of similar length (length = 3.5–4.0 kb, Spearman's $\rho = -0.42$, N = 674; Figure 4E). Similar correlations were also seen for RNAs of other lengths (Figure S3C). By contrast, there was only a small correlation between degradation and RNA length among RNAs with the same number of exons (number of exons = 6, Spearman's $\rho = -0.16$, N = 642; Figure 4F). Again, similar correlations were seen for other exon numbers (Figure S3D). We also tested another

key characteristic of RNAs, guanine-cytosine (GC) content, and found no correlation with PA-X activity in our dataset (Figures S3E and S3F).

The results from the clustering and GO analyses (Figures 3A–3D) suggest that PA-X differentially regulates RNAs from specific functional groups, whereas Figures 4A–4F suggest a difference based on the structure of the nascent transcript. Inter-estingly, we found a connection between the structural and functional specificity. RNAs classified as resistant by *k*-means clustering (shown in Figure 3B) had fewer exons than those classified as PA-X targets (shown in Figure 3A) (Figure 4G). These results suggest that targeting by PA-X is connected to RNA splicing and that this preference has consequences for the selection of functionally relevant targets.

Splice Sites Confer Susceptibility to PA-X

Endogenous RNAs with different numbers of exons also have different sequences, lengths, and post-transcriptional modifications. To investigate the effect of splicing in a more controlled system, we examined the same RNA in both spliced and intronless forms. We used interferon λ2 (IFN-λ2) mRNA as a model transcript. IFN-λ2 is a type III IFN that contributes to IAV immune responses (Jewell et al., 2010). In the RNA-seq, IFN-λ2 transcripts were detectable only in IAV-infected cells and were downregulated by PA-X (Figure S4A). We cloned the IFN-λ2 cDNA and the full IFN-λ2 genomic sequence containing introns into plasmid expression vectors (Figure 5A) and co-transfected them into HEK293T cells with PR8 PA-X. In these transfection experiments, the detection of PA-X protein is hindered by auto-cleavage of the PA-X Pol II transcript. As an alternative control to ensure comparable PA-X activity between transfections, we also measured the RNA levels of a co-transfected intron-containing luciferase reporter (Younis et al., 2010); luciferase downregulation thus serves as a positive control for PA-X activity (Figures 5B–5D, and 5G). We confirmed that IFN-λ2 mRNA was expressed and exported to the cytoplasm at similar levels, irrespective of the construct used (Figures S4B and S4C). We also checked that the 5 introns were properly spliced by PCR analysis (Figures 5E, 5F, and S4D). As expected, we found that PA-X downregulated the IFN-λ2 mRNA expressed from the full genomic region (Figure 5B). However, the levels of the same IFN-λ2 mRNA expressed from an intronless cDNA construct were only minimally reduced (Figure 5B). In both conditions, the control luciferase reporter was downregulated by PA-X, confirming that the activity of PA-X was similar in all of the samples. PA-X proteins from the 2009 pandemic H1N1 strains (e.g., A/California/7/09H1N1 [CA/7] and A/Tennessee/1–560/2009) and the Udorn H3N2 strain also preferentially degraded the spliced mRNAs (Figure 5C). These results confirm the prediction that splicing is important for PA-X targeting. In addition, we tested the downregulation of IFN-λ2 mRNAs expressed from chimeric constructs that contained only 1 of the 5 introns from the original genomic sequence to determine whether a single splicing event was sufficient to restore PA-X targeting. Addition of a single intron increased susceptibility to PA-X (Figure 5D). Downregulation of the luciferase reporter indicated that these changes were not due to varying PA-X activity in the samples. We found that while the addition of introns 1, 3, or 5 alone restored PA-X susceptibility, introns 2 or 4 had little effect. The difference between the introns was also apparent when we normalized IFN-λ2 to luciferase mRNA levels (Figure S4E). Intron 4 was not spliced efficiently in the absence of

other introns (Figure 5E), but intron 2 was still efficiently spliced (Figure 5F). Therefore, splicing efficiency alone does not explain the differential effects of the introns. More in-depth examination of the IFN-λ2 sequence revealed that the 5′ splice sites for introns 1, 3, and 5 match the consensus 5′ splice site sequence, AG|GT (where | marks the splice site). By contrast, the 5′ splice sites for introns 2 and 4 are an imperfect match (TA | GT and GT | GT, respectively). 5′ splice-site quality scores calculated using the MaxEntScan::score5ss program were also higher for introns 1, 3, and 5 (8.8–10.5) than introns 2 and 4 (5.8) (Yeo and Burge, 2004). When we mutated these two 5′ splice sites to match the consensus sequence AG|GT and increase the splice site quality score (mutated introns 2 and 4 = 10.7), we found that the mutated introns 2 and 4 could restore PA-X susceptibility (Figures 5G and S4F normalized to luciferase mRNA levels) and intron 4 splicing efficiency (Figure 5E). This result further strengthens the link between splicing and PA-X susceptibility.

Despite these results linking mRNA splicing and PA-X degradation, one unresolved issue is that we and others have previously used intronless reporters to study PA-X, and they appeared to be efficiently degraded. To investigate this issue, we compared intronless and spliced luciferase reporters (Younis et al., 2010). The spliced reporter, which we used as a control in Figures 5B–5G, contains a portion of the β-globin intron (Younis et al., 2010). PA-X had a more robust effect on the spliced mRNA, although it could also downregulate intronless luciferase mRNA (Figures 5H and S4G). These results suggest that the addition of a single splicing event further promotes degradation by PA-X. Reporter constructs are selected for their robust expression; it is possible that certain intronless reporters also associate with cellular factors involved in PA-X targeting. Never-theless, our findings lead us to recommend the use of intron-containing reporters for future cell-based studies of PA-X.

The X-ORF Mediates Interaction with Proteins Involved in RNA Metabolism

As shown in previous studies (Hayashi et al., 2016; Khaperskyy et al., 2016; Oishi et al., 2015) and the PR8 PA(X9) RNA-seq results (Figure S1B), the C-terminal X-ORF is required for PA-X activity. We hypothesized that the X-ORF interacts with cellular proteins that mediate the association of PA-X with target mRNAs, especially in light of our results connecting PA-X targeting with splicing (Figures 4 and 5) and mRNA 3′ end processing (Khaperskyy et al., 2016). To identify cellular X-ORF-interacting proteins, we used BioID, a proteomic technique that relies on non-specific proximity biotinylation of lysine residues by a modified *Escherichia coli* biotin ligase, BirA* (Roux et al., 2012). Since there are two major classes of PA-X isoforms that differ in X-ORF length (Shi et al., 2012), we fused BirA* to X-ORFs representative of each class: the 61-aa PR8 X-ORF (X61) and the 41-aa CA/7 X-ORF (X41) (Figure 6A). We used BirA* alone and BirA* fused to a mutated PR8 X-ORF in which 4 positively charged residues were replaced by alanine (X61(4A)) as negative controls. These mutations prevent the nuclear localization of a GFP-X-ORF fusion and disrupt mRNA degradation by PA-X (Khaperskyy et al., 2016). As expected from our previous studies (Khaperskyy et al., 2016), fusion to the WT X-ORFs, but not X61(4A), led to the accumulation of BirA* in the nucleus (Figure S5A). Moreover, all BirA* fusions efficiently biotinylated many cellular proteins (Figure S5B).

To identify cellular proteins that bind both the X61 and X41 X-ORFs, we affinity-purified biotinylated proteins from HEK293T cells expressing BirA*-X-ORF fusion proteins and prepared them for quantitative mass spectrometry using reductive dimethylation. Reductive dimethylation exploits formaldehyde variants with different molecular weights due to substituted carbon-13 or deuterium atoms to label captured proteins with stable isotope tags and allow quantitative comparisons among samples (Hsu et al., 2003). We performed the experiment 3 times—twice with BirA*-X61 and once with BirA*-X41—comparing them in each case to the BirA* alone and BirA*-X61(4A) controls (Figure 6A). A total of 156 candidate X-ORF-interacting proteins were represented by at least 2 unique peptides (Table S4) and were present in all of the runs (Figure 6B). Among these, we selected 29 high-confidence interacting proteins with higher relative peptide abundance in the test (BirA*-X61 or -X41) versus control (BirA*-X61(4A) or BirA* alone) conditions (>2-fold higher than controls in at least 2 experiments or >1.5-fold in all 3 experiments; Figure 6D; Table S4). Figure 6C depicts the relative peptide abundance of proteins in X61 samples compared to the X61(4A) control or the BirA* alone control, with black and red open circles identifying the high-confidence hits. Red circles indicate 2 proteins (nucleolin [NCL], nucleophosmin [NPM1]) that were enriched >2-fold compared to controls across all 3 runs. Because NCL and NPM1 are abundant proteins that traffic in and out of nucleoli, these interactions may explain the apparent nucleolar accumulation of biotinylated proteins (Figures S5A and S5C), even though neither the BirA-X-ORF fusion (Figure S5A) nor the full-length PA-X (Khaperskyy et al., 2014, 2016) accumulate in nucleoli. A STRING protein-protein interaction network analysis of the hits revealed several physical and functional interaction nodes, including protein trafficking, transcription, translation, and mRNA processing (Figure 6D). Similarly, GO term analysis revealed a strong association with mRNA processing, RNA splicing, and mRNA metabolic process functions among the high-confidence hits (Figure 6E). These data show that the PA-X C-terminal X-ORF is physically recruited to protein complexes involved in nuclear Pol II RNA processing (commonly referred to as mRNA processing), which likely explains the preferential degradation of RNAs that have undergone co- or post-transcriptional processing.

The CFIm Complex May Regulate PA-X Activity

The BioID screen identified several proteins involved in RNA splicing (RNA binding motif protein 39 [RBM39], poly(U) binding splicing factor 60 [PUF60], and pre-mRNA processing factor 4 [PRPF4]) and/or polyadenylation (nudix hydrolase 21 [NUDT21]/cleavage and polyadenylation specificity factor 5 [CPSF5]/cleavage factor Im 25 [CFIm25] and CPSF6/CFIm68) as X-ORF-interacting proteins. We conducted co-immunoprecipitation experiments to validate these interactions using nuclear extracts derived from an HEK293T iPA-X cell line that produces high levels of a myc-tagged PA-X (Khaperskyy et al., 2016). We recapitulated the interaction between full-length PA-X and endogenous NUDT21, suggesting that this is a stable interaction that can survive affinity isolation procedures (Figures 7A and S6A). NUDT21 and CPSF6 assemble into a functional heterotetrameric CFIm complex (Kim et al., 2010) that enhances polyadenylation and guides polyadenylation site choice (Zhu et al., 2018). In addition, the CFIm complex is present in the spliceosome and has been proposed to link splicing to polyadenylation during RNA processing (Rappsilber et al., 2002; Zhou et al., 2002). To test whether the interaction with the CFIm

complex was required for PA-X activity, we used small interfering RNAs (siRNAs) to deplete NUDT21 and CPSF6 alone or in combination (Figures S6B and S6F). Partial silencing of CFIm proteins reduced PA-X downregulation of IFN-λ2 upon co-transfection in HEK293T cells (Figure 7B). Moreover, in A549 cells, silencing of the CFIm complex reduced PABP nuclear localization during IAV PR8 infection (Figures 7C and 7E), a hallmark of PA-X dependent host shutoff (Figure S2; Khaperskyy et al., 2014). PABP relocalization was quantified on a per-cell basis to control for unrelated effects of the knockdowns on cell viability and infection rates. In fact, we found that NUDT21 silencing reduced cell viability, and CPSF6 silencing dramatically reduced infection rates (Figure 7D). We also tested two additional potential interaction partners, NCL and RBM39, in the PABP relocalization assay (Figures S6C and S6E). While NCL silencing had little effect on cell viability, infection rates, and host shutoff, RBM39 silencing reduced cell viability and infection rates (Figures S6C–S6F). We conclude that NCL is unlikely to have a role in PA-X-mediated host shutoff, whereas the effects of RBM39 silencing on cell physiology are too severe to assess its role in PA-X host shutoff. Nonetheless, these data suggest that the RNA processing and spliceosome-associated CFIm complex is required for at least some of the activity of PA-X in cells.

DISCUSSION

A thorough understanding of the molecular mechanism of action of PA-X is required to determine how it selectively degrades host RNAs and limits innate immune response. In this study, we discovered a key aspect of the PA-X mechanism of action: its selectivity for transcripts that are spliced. This coupling to RNA processing sets PA-X apart from other viral host shutoff RNases that target mRNAs in the cytoplasm in association with translation (Covarrubias et al., 2009; Doepker et al., 2004; Feng et al., 2001, 2005; Gaglia et al., 2012; Kamitani et al., 2009). Our transcriptomic results show that, as expected, PA-X downregulates many host RNAs, both on its own and in the context of infection. However, some RNAs are less susceptible to PA-X activity, and a key characteristic of these resistant RNAs is that they are intronless or have fewer introns. Moreover, the C-terminal X-ORF of PA-X interacts with many proteins involved in cellular RNA metabolism. We propose a model whereby PA-X associates with a discrete set of RNA metabolism proteins that allows selective targeting of RNAs during transcription or early processing. In this model, RNAs that are not canonically processed, including viral RNAs, are spared.

Our transcriptomic study confirms that the PA-X-dependent downregulation of host protein production (Hayashi et al., 2015; Jagger et al., 2012) is due to a reduction in RNA levels, and defines PA-X-dependent and PA-X-independent components of RNA downregulation during infection. The PA-X-independent component is likely due to a recently described generalized reduction in cellular transcription (Bauer et al., 2018; Heinz et al., 2018; Zhao et al., 2018), because other known modalities of IAV host shutoff are not active in the PR8 strain (Das et al., 2008; Rodriguez et al., 2009; Salvatore et al., 2002). The mechanism of reduced host transcription in IAV-infected cells remains a matter of debate (Bauer et al., 2018; Heinz et al., 2018; Zhao et al., 2018). However, it is most likely PA-X independent, because transcription is also reduced during infection with influenza B viruses (Bauer et al., 2018), which do not encode PA-X (Shi et al., 2012). Our clustering analysis also revealed

that some functional classes of RNAs are spared from PA-X degradation, including mRNAs for proteins involved in translation, which agrees with previous results from Bercovich-Kinori et al. (2016) (Figure 3D). Our new results suggest that the small number of exons of these mRNAs, particularly RNAs for ribosomal proteins, may explain this phenomenon.

Another general conclusion of our RNA-seq analysis is that PA-X with a 9-aa truncated C-terminal X-ORF is essentially non-functional in the context of infection. The shutoff impairment of IAV PA(X9) is very similar to that of the PA(fs) and PA(ΔX) viruses (Figure S1B), which presumably have reduced PA-X production. This finding validates the results of multiple studies using ectopic PA-X expression models that concluded that at least 15 aa of the X-ORF is required for full RNA degrading activity in cells (Hayashi et al., 2016; Khaperskyy et al., 2016; Oishi et al., 2015), despite *in vitro* activity of the RNase domain in isolation (Bavagnoli et al., 2015; Dias et al., 2009; Yuan et al., 2009). Similarly, a 1918 H1N1 chimeric virus with a stop codon after 15 aa had an intermediate host shutoff phenotype between IAV WT and PA(fs) (Jagger et al., 2012). The finding that truncating the X-ORF is sufficient to block PA-X activity in the virus is important because single-point mutations in the X-ORF sequence are less disruptive than frameshifting mutations. Thus, viruses carrying X-ORF mutations could be better tools for *in vivo* studies of PA-X function and IAV pathogenesis.

The key unexpected finding from our study is the link between PA-X and splicing. All other viral host shutoff RNases appear to act at some stage of mRNP loading into the translation apparatus. For example, RNA targeting by the alphaherpesvirus protein vhs is linked to physical interactions with translation initiation factors (Doepker et al., 2004; Feng et al., 2001, 2005) and SARS CoV nsp1 only degrades RNAs that are actively translated (Gaglia et al., 2012; Kamitani et al., 2009). Thus, to our knowledge, there is no other described instance of a host shutoff RNase using splicing as a targeting mechanism. In fact, splicing was reported to protect mRNAs from cleavage by vhs (Sadek and Read, 2016). The connection between splicing and PA-X degradation is evident from the reduced effect of PA-X on intronless mRNAs (Figures 4 and 5), the negative correlation between exon number and degree of degradation by PA-X (Figures 4 and S3), and the fact that small changes in the 5′ splice site can affect the susceptibility to degradation by PA-X (Figures 5G and S4F). These findings begin to shed light on the specificity of PA-X for Pol II transcripts (Khaperskyy et al., 2016). In cellular transcription, the splicing machinery associates with RNAs through interactions with Pol II, and thus only Pol II transcripts are normally spliced (Gu et al., 2013). Protein-protein interactions with splicing factors may thus bring PA-X to its Pol II targets. This idea is corroborated by our proteomic analysis, which shows that the PA-X X-ORF interacts with several splicing regulators (PUF60, RBM39, PRPF4) and spliceosome-associated polyadenylation proteins (the CFIm complex proteins NUDT21 and CPSF6) (Figure 6). Furthermore, PA-X activity is in part dependent on the CFIm complex (Figure 7). We speculate that more exons provide more chances for PA-X to be brought to the RNA by these factors, resulting into more efficient turnover of RNAs with more splice sites. Since these proteins do not regulate the processing of all of the mRNAs in the cell to the same extent, PA-X interactions with these proteins could provide an additional mechanism for target discrimination. Further studies will be needed to determine the exact role of these factors.

A targeting strategy based on splicing offers a major benefit to the virus because it provides the ability to easily discriminate between host and viral mRNAs. Viral mRNAs are synthesized by the RdRp, and most of them are not spliced, which renders them “invisible” to PA-X. That said, our published results suggest that even the two viral mRNAs that are spliced (nuclear export protein [NEP] and matrix protein 2 [M2]) are PA-X resistant (Khaperskyy et al., 2016). However, splicing of viral mRNAs is a fundamentally different process, since the splicing machinery needs to be recruited to the RNAs separately from Pol II (Dubois et al., 2014). It is possible that viral mRNA splicing does not require the CFIm complex or other PA-X-binding partners, because they are auxiliary components of the host RNA processing machinery. The PA-X splicing-based targeting strategy is more efficient at virus versus host discrimination than the translation-based targeting strategy used by herpesviral host shutoff RNases, which leads to the degradation of viral and host mRNAs alike (Abernathy et al., 2014). This is likely because viral translation relies on the same machinery as host translation. While herpesviruses can compensate for the degradation of their own RNAs, this self-sacrifice may not work for a virus such as IAV, which has a shorter replication cycle and a small genome with a limited gene expression program.

Our BioID results suggest that the preference for spliced RNAs may be linked to protein-protein interactions between the PA-X X-ORF and cellular factors. The X-ORF is required for PA-X nuclear localization (Hayashi et al., 2016; Khaperskyy et al., 2016; Oishi et al., 2015). However, enforced nuclear localization of the PA-X RNase domain alone does not fully rescue activity (Hayashi et al., 2016), suggesting that the X-ORF has additional functions. We identified many X-ORF-interacting proteins with various roles in RNA metabolism in addition to a nuclear import protein (import in 7 [IPO7]). By examining the X-ORF in isolation, we likely excluded indirect interactions via RNA binding of the RNase domain, as well as interactions that are important for PA rather than PA-X function. Among our hits, two nucleolar proteins, NCL and NPM1, were also reported to interact with H5N1 PA-X (Li et al., 2016). The fact that biotinylated proteins accumulated in the nucleoli also supports the idea that NCL and NPM1, which traffic to nucleoli, come in contact with the BirA*-fused X-ORF and full-length PA-X (Figure S5C). It is unclear whether PA-X interaction with nucleolar proteins is of functional importance, since silencing NCL had little effect on PA-X-mediated host shutoff in infected cells (Figures S6C–S6F) and PA-X is not localized specifically to this compartment (Figure S5A; Khaperskyy et al., 2014, 2016). NCL has been reported to protect specific RNAs from degradation by viral host shutoff RNases, including PA-X (Muller and Glaunsinger, 2017; Muller et al., 2015). Therefore, the PA-X-NCL interaction may reflect a different role for NCL in regulating RNA homeostasis during infection. By contrast, we found evidence for the involvement of the CFIm complex (NUDT21 and CPSF6) in host shutoff during infection (Figures 7D and 7E) and PA-X ectopic expression (Figure 7B). The findings in infected cells must be interpreted with caution because CPSF6 silencing markedly inhibited viral infection (Figures 7D, 7F, and S6F). It is unclear whether the reduction in infection rates is connected to PA-X function. While the CFIm complex is more commonly studied for its roles in alternative polyadenylation and mRNA 3′ processing (Hardy and Norbury, 2016), multiple studies have shown that NUDT21 and CPSF6 are found in purified spliceosome complexes (Rappsilber et al., 2002; Zhou et al., 2002). This finding has led to the idea that they may also play a role in

the coordination of splicing and 3′ processing (Martinson, 2011). In a previous study, we reported that canonical 3′ end processing may also be linked to PA-X targeting (Khaperskyy et al., 2016); the CFIm complex may also explain this connection. Little is known about the function of the CFIm complex, so studying its contribution to PA-X activity and/or IAV infection may advance the understanding of its normal physiological role. Roles for the other candidate PA-X-interacting proteins remain to be explored; such studies may be hindered if these proteins play PA-X-independent roles in the viral replication cycle or in maintaining general cell viability during infection. For example, we found that silencing RBM39, an alternative splicing regulator, had profound negative effects on cell survival and infection rates (Figures S6D–S6F). We also wonder whether the association of PA-X with cellular proteins could compromise their normal function. We did not find dramatic changes in host splicing in our dataset (not shown), but others have reported increased intron retention in cells infected with a PR8 chimeric virus bearing a 1918 NS1 protein (Zhao et al., 2018). This discrepancy could be due to the way we set up our sequencing pipeline or to the NS1 variant present in the virus. Because these changes were attributed to NS1 activity, we must be cautious in our assessment of PA-X-dependent and PA-X-independent effects in our system.

It is interesting that both PA-X and the well-known influenza host shutoff factor NS1 interact with nuclear mRNA processing machinery to control gene expression (Nemeroff et al., 1998). Many NS1 variants (but not PR8 NS1) cause host shutoff by binding and inhibiting a component of the 3′ end RNA processing machinery, CPSF30 (Das et al., 2008; Nemeroff et al., 1998). While this convergence could allow the two proteins to coordinate an attack on the host, studies of engineered and naturally evolved viruses suggest that NS1 and PA-X activities are anti-correlated to prevent cytotoxicity. For example, the original 2009 pandemic H1N1 NS1 does not bind CPSF30, nor does it reduce host gene expression (Hale et al., 2010), but the more human-adapted NS1 from currently circulating pandemic H1N1 strains does (Clark et al., 2017; Nogales et al., 2018). These H1N1 strains have also accumulated mutations that reduce PA-X activity, suggesting that having two highly active host shutoff proteins may impair viral fitness (Nogales et al., 2018). A recent study by the Takimoto lab comparing NS1 and PA-X targeting in a 2009 pandemic strain suggests that NS1 and PA-X have overlapping but not identical targets (Chaimayo et al., 2018). NS1 is more clearly directed at downregulation of the innate immune response, whereas PA-X has a broader targeting range (Chaimayo et al., 2018). In general, host mRNA processing may be a hub of regulation for influenza because viral mRNAs are generally not processed by host machinery. Also, interactions with host mRNA processing do not directly compromise Pol II activity, which is required for viral replication (Lamb and Choppin, 1977).

Our results affirm the importance of PA-X for the viral replication cycle, as they show that the ability of the virus to regulate host gene expression is severely reduced in the absence of PA-X. Moreover, we have uncovered a unique mechanism of host RNA targeting that can allow PA-X to distinguish not only between host and viral targets but also among cellular targets. For example, the intronless mRNA TAF7, which we examined in Figures 2B and 2C, is a component of Pol II pre-initiation complexes. Therefore, PA-X selectivity could have repercussions for the viral replication cycle. Through further elucidation of the PA-X mechanism of action, we will gain important insights into how host shutoff allows the virus

to usurp host biosynthetic machinery and expand our knowledge of the link between PA-X and IAV pathogenesis.

STAR★METHODS

CONTACT FOR REAGENT AND RESOURCE SHARING

Further information and request for resources and reagents should be directed to and will be fulfilled by the Lead Contact, Marta M. Gaglia (Marta.Gaglia@tufts.edu).

EXPERIMENTAL MODEL AND SUBJECT DETAILS

Cell lines—Human embryonic kidney cells HEK293A (Thermo Fisher) and HEK293T (ATCC), and human adenocarcinoma alveolar basal epithelial (A549, ATCC) cells were obtained from commercial sources. HEK293A and HEK293T are female and A549 are male. All cell lines and derivatives were cultured in Dulbecco's modified Eagle's medium (DMEM) supplemented with 10% fetal bovine serum (Hyclone) at 37°C and 5% CO_2. HEK293T_iPA-X-PR8, A549-iPA-X_PR8 and A549-iPA-X-D108A_PR8 were previously described (Khaperskyy et al., 2016). A549-iPA-X_Udorn and iPA-X_PR8_Nterm were generated by transducing A549 cells with lentiviruses containing pTRIPZ-PA-X_Udorn-myc and pTRIPZ-PA-X_PR8-Nterm-myc.

METHOD DETAILS

Plasmids—pCR3.1-PA-X-myc (with PR8 PA-X) (Khaperskyy et al., 2014), pCR3.1-PA-N191 (PA-X 0 aa) (Khaperskyy et al., 2016), pCR3.1- PA-X_TN/CA/7-myc (Khaperskyy et al., 2016), pd2GFP-HR (Lee and Glaunsinger, 2009), pCDNA3.1-β-globin ((Covarrubias et al., 2011), subcloned from the pcTet2-bwt plasmid (Singh et al., 2008)) were previously described. The luciferase constructs with and without the intron were a kind gift from Gideon Dreyfuss (Younis et al., 2010). pHW-PA(X9) and pHW-PA(ΔX) were generated from pHW-193 (kind gift from R. Webby) and pHW-PA(fs) vectors (Khaperskyy et al., 2016), respectively, using Phusion site-directed PCR mutagenesis to introduce the TAG stop codon in +1 ORF (synonymous ATT to ATA substitution at PA Ile-201 codon, TTG to TAG substitution at PA-X Leu-201). pCR3.1-PA-X_9aa-myc and pCR3.1-PA-X_15aa-myc were generated from the pCR3.1-PA-X-myc constructs by amplifying the truncated coding region and inserting it into the SalI-MluI sites of a pCR3.1-C-terminal-myc backbone. pCR3.1-PA-X_Udorn-myc was generated by PCR amplifying the 5′ portion of the segment 3 RNA from a PolI-Udorn construct (kind gift from A. Mehle), adding a single nucleotide deletion to shift the frame of the X-ORF, and inserting into the SalI-MluI sites of a pCR3.1-C-terminal-myc backbone. pTRIPZ-PA-X-Nterm-myc and pTRIPZ_PA-X_Udorn-myc were generated by PCR amplifying PA-N191 from pCR3.1-PA-N191-myc and PA-X-Udorn-myc from pCR3.1-PA-X_Udorn-myc, respectively, and inserting these sequences into the backbone of pTRIPZ-RFP_SV40_3′UTR (Khaperskyy et al., 2016) after RFP excision with AgeI and ClaI. pCMV-IFN-λ2 cDNA, genomic and single intron constructs were generated by PCR amplifying the full human IFN-λ2 cDNA, the genomic locus, or combinations of fragments of the two, and inserting into the pd2eGFP-N1 construct (Clontech) after the GFP was excised using NheI and NotI. The 5′ splice site of intron 2 or 4 was then mutated from TTA|GT and TGT|GT, respectively, to CAG|GT within the single-intron constructs to generate the

intron 2 and 4 mutant constructs. Gibson cloning using HiFi assembly mix (New England Biolabs) was used to make all of these constructs, unless otherwise stated. The expression vector for the biotin ligase from *E. coli* with the R118G mutation BirA* (pcDNA3.1-myc-BioID2-MCS) (Roux et al., 2012) was obtained from Addgene (#74223) and the BirA* ORF was amplified by PCR and inserted into the pCR3.1-myc vector (Khaperskyy et al., 2012) between KpnI and EcoRI sites to generate pCR3.1-BirA*-myc. The PCR-amplified X-ORF sequences from pCR3.1-PA-X-myc and pCR3.1-PA-X(4A)-myc (Khaperskyy et al., 2016) were inserted in frame with BirA* ORF using EcoRI and MluI to generate pCR3.1- BirA*-X61-myc and pCR3.1-BirA*-X61(4A)-myc, respectively. X-ORF coding sequence from A/California/7/2009 H1N1 strain was amplified from pHW-C3 vector (Slaine et al., 2018) and inserted in frame with BirA* ORF using EcoRI and XhoI to generate pCR3.1-BirA*-X41(CA/7) vector.

Cell lines, lentiviral transduction and transfections—HEK293A, HEK293T, A549 cells and derivatives were cultured in Dulbecco's modified Eagle's medium (DMEM) supplemented with 10% fetal bovine serum (Hyclone) at 37°C and 5% CO_2. HEK293T_iPA-X-PR8, A549-iPA-X_PR8 and A549-iPA-X-D108A_PR8 were previously described (Khaperskyy et al., 2016). A549-iPA-X_Udorn and iPA-X_PR8_Nterm were generated by transducing A549 cells (ATCC) with lentiviruses containing pTRIPZ-PA-X_Udorn-myc and pTRIPZ-PA-X_PR8-Nterm-myc. Lentiviral packaging was carried out using the packaging plasmids psPAX2 and pMD2.G (Addgene #12260, #12259). For experiments using iPA-X cells, cells were treated with 0.2 mg/ml doxycycline for 18 h to induce PA-X expression prior to RNA or protein sample collection. For the RNaseq experiments, untransduced A549 cells were also treated with doxycycline to serve as the control. For experiments using IFN-λ2 constructs and the β-globin reporter, HEK293T cells were plated in 24-well or 6-well plates (for fractionation experiments) and transfected with 800 ng/ml total DNA (including 50 ng/ml PA-X construct) using polyethylenimine (PEI). Cells were collected 24 h later for fractionation and/or RNA extraction and purification, and cell lysates for western blot. For siRNA transfections, HEK293T cells were plated in 6-well plates while transfecting 15 nM siRNA (ThermoFisher Scientific) per well using Lipofectamine RNAiMAX reagents (ThermoFisher Scientific). Cells were transfected two days later with 800 ng/ml total DNA (including 50 ng/ml PA-X construct) using PEI, and collected for RNA and protein 24 h later.

Viruses and infections—Wild-type influenza A virus A/Puerto Rico/8/1934 H1N1 (PR8) and the mutant recombinant viruses PR8 PA(X9), PR8 PA(fs) and PR8 PA(ΔX) were generated using the 8-plasmid reverse genetic system (Hoffmann et al., 2000) as previously described (Khaperskyy et al., 2012). Viral stocks were produced in MDCK cells and infectious titers determined by plaque assays in MDCK cells using1.2% Avicel overlays as described in Matrosovich et al. (Matrosovich et al., 2006). A549 cell monolayers were mock-infected or infected with the wild-type or mutant viruses at MOI = 1 for 1 h at 37°C. Then monolayers were washed briefly with PBS, fresh infection media (0.5% BSA in DMEM supplemented with 20 μM L-glutamine) was added and cells incubated at 37°C in 5% CO_2 atmosphere for 12 or 15 h prior to RNA isolation or preparation of lysates for western blotting. For immunofluorescence microscopy analysis cells grown on glass

coverslips were infected as described above and fixed at 15 h post-infection using 4% paraformaldehyde in PBS.

Preparation of cell lysates containing biotinylated proteins—HEK293T cells grown on 10-cm dishes were washed briefly and transfected with BirA* fusion protein expression constructs using PEI. At 6 h post transfection, media was changed to 10% FBS DMEM supplemented with 50 μM biotin (Sigma). 24 h post-transfection (18 h post-biotin addition) cells were washed and collected in ice cold PBS, and centrifuged at 250 × *g* for 5 min at 4°C. Cell pellets were resuspended in 500 μl RIPA buffer (50 mM Tris-HCl pH 7.4, 150 mM NaCl, 1% Igepal, 0.5% sodium deoxycholate, 0.1% SDS) with protease inhibitor cocktail (P8340, Sigma) and lysed at 4°C for 1 h with gentle agitation, followed by passing through a 21-gauge needle. Lysates were cleared by centrifugation at 4°C for 20 min at 20,000 × *g*.

Neutravidin pull-down—60 ml of 50% slurry of High Capacity Neutravidin Agarose Beads (Thermo) was used for each 500 μl of clarified whole cell lysate. Beads were equilibrated in RIPA buffer by washing three times for 10 min at 4°C. In one of the BirA*-X61 experimental runs, 1 μl of 500x RNase A (100 mg, QIAGEN) was added to each sample to remove non-specific interactors. The lysate was then incubated for 5 min at room temperature before loading onto the beads. Untreated samples were loaded directly onto the beads post washing. 1 mg of protein sample was loaded to beads in 1.5 ml Eppendorf tubes, which were then placed on a rotator overnight at 4°C, and collected with centrifugation at 400 × *g* for 1 min at 4°C. Beads were washed with RIPA buffer three times, followed by three washes with TAP buffer (50 mM HEPES-KOH pH 8.0, 100 mM KCl and 10% glycerol).

Mass spectrometry sample preparation—Beads were resuspended in 50 mM triethylammonium bicarbonate (TEAB) buffer (Sigma). 24 mM DTT and 32 mM IAcNH2 were added sequentially. Beads were then incubated for 30 min at 37°C, washed with 50 mM TEAB and centrifuged for 1 min at 400 × *g* before resuspending in 50 mM TEAB. On-bead trypsin (Pierce Trypsin protease, MS-Grade; Thermo Scientific) digest was performed with 1 μg trypsin in 50 mM TEAB buffer, shaken overnight at 37°C. Samples were acidified with 1 μl trifluoroacetic acid (TFA) and 3 μl Formic acid until a pH lower than 3 was achieved. Trypsinized peptides were collected by puncturing a hole in the bottom of the 1.5 ml Eppendorf tube using a 30-gauge needle, placing it in a 2 ml Eppendorf tube and spinning it at 2000 rpm for 1 min at room temperature. Beads were washed with 50 mM TEAB prior to desalting. Samples were desalted with Oasis/SepPak Desalting columns, eluted sequentially in 1 ml 50% ACN/0.1% TFA and 500 μl 70% ACN/0.1% TFA. Combined eluted samples were dried in a Thermo SPDIIIV speed vacuum centrifuge and frozen at −20°C.

Reductive dimethylation and quantitative mass spectrometry—Quantitative mass spectrometry analysis via reductive dimethylation enabled measurements of relative abundance of biotinylated proteins in each experimental condition (Hsu et al., 2003). In reductive dimethylation, formaldehyde molecules with different combinations of stable

hydrogen and carbon isotopes are conjugated to peptide samples. Dried protein samples were resuspended by sonication for 15 min in 50 mM TEAB. BirA*, BirA*-XORF (X61 or X41) and BirA*-X61(4A) samples were labeled with light, medium and heavy isotopes respectively. 8 μl formaldehyde (Sigma) were added to the light, 15 μl D2-formaldehyde (Cambridge Isotope Laboratories Inc.) to the medium and 15 μl D2-C13-formaldehyde (Aldrich) to the heavy samples. Reactions were incubated for 5 min at room temperature. Once incubation was completed, 0.51 M $NaCNBH_3$ (sodium cyanoborohydride; Fluka) was added to the light and medium samples, while 0.51 M $NaCNBD_3$ (sodium cyanoborodeuteride; Aldrich) was added to the heavy reaction, to label terminal amines. All three reactions were incubated for 1 h at room temperature before being combined into a single tube at a 1:1:1 ratio. The combined sample was acidified, desalted and dried as described above. Samples were resuspended in 3% ACN/0.1% formic acid and sonicated for 15 min to prepare for mass spectrometry. Mass spectrometry and peptide identification was performed at Dalhousie Proteomics CORE Facility by Dr. Alejandro Cohen (https://medicine.dal.ca/research/mass-spectrometry-proteomics-and-metabolomics.html). Proteome Discoverer software (Thermo) was used for protein identification. Functional Protein Association Network analysis was conducted on 29 selected protein hits using online STRING version 10.5 (https://string-db.org/) (Szklarczyk et al., 2017).

Cell fractionation for RNA analysis—Fractionation was performed as described previously (Gagnon et al., 2014) with minor modifications. Briefly, cells were collected 24 h after transfection, centrifuged at 500 × *g* for 5 min at 4°C, then washed with PBS and counted. Equal numbers of cells were aliquoted into two tubes, one for the whole cell lysates collection and one for fractionation. Cells were pelleted again, and lysed on ice for 10 min in 250 μl ice-cold hypotonic lysis buffer (10 mM Tris pH 7.5, 10 mM NaCl, 3 mM $MgCl_2$, 0.3% (vol/vol) NP-40, 10% (vol/vol) glycerol in nuclease-free water) supplemented with 100 U RNasin (Promega). For the whole cell lysate, Trizol (Life Technologies) was added directly to the lysate to extract RNA. For nuclear/cytoplasmic fraction, the lysate was centrifugated at 1000 × *g* for 3 min at 4°C to pellet membrane and nuclei. The supernatant was collected as the cytoplasmic fraction and Trizol was added to it to extract RNA. Finally, the nuclear pellet was washed 3 times with 1 ml hypotonic lysis buffer and collected by centrifugation at 200 × *g* for 2 min at 4°C, then lysed directly in Trizol to extract nuclear RNA.

RNA purification, cDNA preparation and qPCR—For fractionation experiments, RNA was purified using Trizol. 1 ml Trizol, 2 μl glycogen and 200 μl chloroform (Fisher Scientific) were added to each fraction. Samples were then centrifuged at 16,000 × *g* for 15 min at 4°C, and the aqueous layer was collected. RNA was precipitated by addition of 700 μl isopropanol and incubation for 10 min at room temperature, followed by centrifugation at 16,000 × *g*, 4°C for 20 min. The pellet was washed with 75% ethanol, and resuspended in RNase-free water. For other transfection experiments, RNA was extracted from cells and purified using the Quick-RNA miniprep kit (Zymo Research), following manufacturer's protocol. In all cases, the RNA was treated with Turbo DNase (Life Technologies), then reverse transcribed using iScript supermix (Bio-Rad) per manufacturer's protocol. In the fractionation experiment, the same cell equivalents of total, nuclear and cytoplasmic fraction

were used for these steps. qPCR was performed using iTaq Universal SYBR Green supermix (Bio-Rad), on the Bio-Rad CFX Connect Real-Time System qPCR and analyzed with Bio-Rad CFX Manager 3.1 program. The primers used are listed below.

Intron splicing verification—Proper splicing of each intron for all IFN-λ2 construct was verified by PCR amplification across each splice sites using primers listed below. PCR products were run on a 2% agarose gel containing HydraGreen safe DNA dye (ACTGene) and imaged with a Syngene G:Box Chemi XT4 gel doc system.

Co-immunoprecipitation from nuclear lysates—HEK293T_iPA-X-PR8 cells were plated in 10-cm dishes. Cells were then treated with 1 μg/ml doxycycline for 18 h to induce PA-X expression. Fractionation of nuclear lysates was performed as described previously (Dadi et al., 2013) with minor modifications. Briefly, cells were washed with ice-cold Dulbecco's PBS and centrifuged at 1,200 rpm for 6 min at 4°C to collect the cells. Cell pellets were lysed in 50 μl of a sucrose-based lysis buffer (0.32 M sucrose, 3 mM $CaCl_2$, 2 mM MgOAc, 0.1 mM EDTA, 10 mM DTT, 0.5 mM PMSF). An additional 50 ml of sucrose lysis buffer with 0.5% (vol/vol) NP40 was added to the lysate. The lysate was centrifuged for 10 min at 1,100 × *g* at 4°C. The supernatant was collected as the cytoplasmic fraction, whereas the pellet was washed in 100 μl of sucrose lysis buffer, and centrifuged for 10 min at 2,000 rpm at 4°C. The supernatant was discarded and the pellet was lysed in 100 μl of Soluble Nuclear Lysis Buffer (50 mM HEPES pH 7.8, 50 mM KCl, 300 mM NaCl, 0.1 mM EDTA, 10% Glycerol, 1 mM DTT, 0.1 mM PMSF, cØmplete protease inhibitors (Roche)) and incubated on a rotating rotor at 4°C for 45 min. Samples were centrifuged at 10,000 × *g* for 3 min at 4°C. 20 μl of the supernatant was collected as the input sample, and the rest was added to myc-trap magnetic agarose beads (ChromoTek), or control magnetic agarose beads (ChromoTek) and incubated on a rotating rotor for 45 min at 4°C. Beads were collected on a magnetic rack and washed 6 times with wash buffer (50 mM Tris HCl pH 7.4, 150 mM NaCl, 1 mM EDTA, 0.05% NP40, cØmplete protease inhibitors (Roche)). 25 μl of Laemmli sample buffer was added to the beads, and samples were incubated for 10 min at 95°C prior to SDS-PAGE and western blotting.

Western blotting and immunofluorescence—Western blotting and immunofluorescence were carried out as previously described (Khaperskyy et al., 2014, 2016) using the antibodies listed in the Key Resources Table. For detection of biotinylated proteins, HRP-conjugated streptavidin (Cell Signaling) and Alexa Fluor-488-conjugated streptavidin (Molecular Probes) were used.

RNA-seq—For RNA-seq analysis of PA-X-expressing cells, A549 and A549 iPA-X cells were induced with 0.2 μg/ml doxycycline for 18 h. For RNA-seq analysis of infected cells, A549 cells were infected with PR8 wt, PA(fs), PA(X9), and PA(ΔX) viruses or mock infected for 15 h. Each condition was tested at least twice. RNA lysates were collected and purified using the RNeasy kit (QIAGEN). 650–750 ng of RNA were mixed with ERCC ExFold RNA spike-in mix (0.65 μl or 0.75 μl, respectively, Invitrogen/ThermoFisher) prior to the start of library preparation. The spike-in controls were included to better normalize the final RNA levels. This particular kit contains two mixes that can be used for the control

versus test samples and that have known fold change differences. This information can be used to re-calibrate the samples. Prior to library preparation, the levels of select human mRNAs were tested by RT-qPCR, to confirm that PA-X overexpression/IAV infection had the expected effect. Libraries were prepared using the TruSeq Stranded Total RNA Library Prep Kit with Ribo-Zero Human (Illumina) following the manufacturer's protocol. Library preparation was evaluated using a Fragment Analyzer (Advanced Analytical Technologies, Inc.) at the Tufts University Core Facility - Genomics Core. High-throughput sequencing was carried out by the Tufts Genomics facility on a HiSeq 2500. Single-end 50 nucleotide reads were obtained with a multiplexing strategies, using a total of four lanes. For the replicates, the spike mixes for the samples and the barcoded primers were switched, in order to control for potential biases.

Read alignment and bioinformatic analysis—Reads were aligned with Tophat2 v2.1.1 (Kim et al., 2013) to hg19, IAV PR8 and the ERCC spike sequences. Default settings were used, except --library-type fr-firststrand, and a gtf of the hg19 annotation was provided as reference. Table S1 summarizes the results of the alignment. FPKMs were computed using Cufflinks v2.2.1 (Trapnell et al., 2012). Default settings were used, except --library-type fr-firststrand and –u, and a gtf of the hg19 annotation was provided as reference. Only previously annotated RNAs with a level of >1 FPKM in all the control samples (A549 + dox or mock-infected A549) were used in further analyses. Because most annotated RNAs are Pol II transcripts, the downstream analysis includes predominantly Pol II transcripts. The FPKMs for the RNAs were converted to attomoles of RNA based on the known concentration of the spike-in controls. Table S2 shows the high correlation in measured RNA levels between replicate samples. The absolute RNA levels in the replicates were averaged, and the relative RNA levels (RNA ratio) in infected versus mock infected or PA-X-expressing versus control cells was computed. All downstream analysis was carried out on the relative levels (ratio) in log2 scale. Data S1 and S2 include tables that summarize the results of the RNaseq analyses. The hg19 annotation was used to derive the number of exons, length of transcripts and GC content for the analyses in Figures 4, S3. For analysis of intronless RNAs, only RNAs that were longer than 300 nt were used, to enrich for mRNAs and long non-coding RNAs and exclude small non-coding RNAs that are transcribed by Pol III or are produced through processing of longer transcripts, like microRNAs and small nuclear and nucleolar RNAs. The length distribution of the remaining intronless RNAs was similar to that of the spliced RNAs. All RNAs were used for the analysis of PA-X downregulation versus length, exon number, and GC content. *k*-means clustering analysis was carried out using the Cluster 3.0 program (http://bonsai.hgc.jp/~mdehoon/software/cluster/software.htm). The clustering was done only on RNAs that were detected in all samples tested (6,391 RNAs), because all eight datasets were used to generate the clusters, even though only the mRNA levels for select samples are plotted in Figures 3A–C for clarity. The classified RNAs listed in Data S1a, S1b, S1c and S2a, S2b, S2c represent these 6,391 RNAs. Because in *k*-means clustering the number of clusters is user-defined, clustering was attempted with three, four, and five clusters. Four clusters were chosen, because they provided more granularity. For example, they identified a group of RNAs that were only PA-X-dependent in the ectopic expression system. Initializing the program with more than four clusters led to separation of PA-X targets in multiple groups different only by

the extent of downregulation, but did not identify other patterns of gene expression. Gene ontology (GO) term analysis was carried out on the DAVID server (Huang et al., 2009a, 2009b). The 5′ splice site quality score was computed using the MaxEntScan::score5ss program using the maximum entropy model (Yeo and Burge, 2004). Other analyses were done using custom scripts in Python2.7. For the ISG analysis (Figure 3E) the list of ISG tested by Schoggins et al. was used (Schoggins et al., 2011).

QUANTIFICATION AND STATISTICAL ANALYSIS

For Figures 1B, 2C, 5, 7, S4, S6, statistical analysis and plotting were done in GraphPad Prism v7.0d software using the test recommended by the software and indicated in the figure legends. Generally, ANOVA followed by a corrected pairwise test (Tukey's or Dunnett's) was used when more than two samples were analyzed and Student's t test when two samples were compared. For Figures 1C and 1D, 2A and 2B, 4, statistical analysis and plotting were done using Python2.7 and the NumPy, SciPy and matplotlib libraries. The Kolmogorov-Smirnoff test was used to compare populations and Spearman's correlation coefficient to analyze the relationship between certain variables and RNA downregulation. Statistical tests used for each panel are noted in Figure legends and/or Figures.

DATA AND SOFTWARE AVAILABILITY

The accession number for the RNA-seq data reported in this paper is GEO: GSE120183 (raw read data and processed data included here as Data S1 and S2).

Supplementary Material

Refer to Web version on PubMed Central for supplementary material.

ACKNOWLEDGMENTS

We thank Albert Tai and the personnel of the Tufts University Core Facility - Genomics Core for help with the RNA-seq. We thank Alejandro Cohen of the Dalhousie Proteomics and Mass Spectrometry Core Facility for support of the BioID proteomics analysis. We thank Andrew Mehle and Richard Webby for constructs, Claire Moore and Andrew Bohm for suggestions and feedback, and members of the Gaglia and McCormick labs for critical reading of the manuscript. This work was supported by a Natalie V. Zucker award from Tufts University (to M.M.G.), NIH grant R01 AI137358 (to M.M.G.), and Canadian Institutes for Health Research grant MOP-136817 (to C.M.). L.G. was supported by NIH training grant T32 GM007310. R.E.L. and Y.K. were supported by NIH training grant T32 AI007422. C.H.R. was partially supported by the Applied Mathematics Program of the US Department of Energy (DOE) Office of Advanced Scientific Computing Research under contract number DE-AC02–05CH11231.

REFERENCES

Abernathy E, Clyde K, Yeasmin R, Krug LT, Burlingame A, Coscoy L, and Glaunsinger B (2014). Gammaherpesviral gene expression and virion composition are broadly controlled by accelerated mRNA degradation. PLoS Pathog. 10, e1003882. [PubMed: 24453974]

Abernathy E, Gilbertson S, Alla R, and Glaunsinger B (2015). Viral Nucleases Induce an mRNA Degradation-Transcription Feedback Loop in Mammalian Cells. Cell Host Microbe 18, 243–253. [PubMed: 26211836]

Ank N, West H, Bartholdy C, Eriksson K, Thomsen AR, and Paludan SR (2006). λ interferon (IFN-λ), a type III IFN, is induced by viruses and IFNs and displays potent antiviral activity against select virus infections in vivo. J. Virol 80, 4501–4509. [PubMed: 16611910]

Arias C, Weisburd B, Stern-Ginossar N, Mercier A, Madrid AS, Bellare P, Holdorf M, Weissman JS, and Ganem D (2014). KSHV 2.0: a comprehensive annotation of the Kaposi's sarcoma-associated herpesvirus genome using next-generation sequencing reveals novel genomic and functional features. PLoS Pathog. 10, e1003847. [PubMed: 24453964]

Bauer DLV, Tellier M, Martínez-Alonso M, Nojima T, Proudfoot NJ, Murphy S, and Fodor E (2018). Influenza Virus Mounts a Two-Pronged Attack on Host RNA Polymerase II Transcription. Cell Rep. 23, 2119–2129.e3. [PubMed: 29768209]

Bavagnoli L, Cucuzza S, Campanini G, Rovida F, Paolucci S, Baldanti F, and Maga G (2015). The novel influenza A virus protein PA-X and its naturally deleted variant show different enzymatic properties in comparison to the viral endonuclease PA. Nucleic Acids Res. 43, 9405–9417. [PubMed: 26384413]

Bercovich-Kinori A, Tai J, Gelbart IA, Shitrit A, Ben-Moshe S, Drori Y, Itzkovitz S, Mandelboim M, and Stern-Ginossar N (2016). A systematic view on influenza induced host shutoff. eLife 5, e18311. [PubMed: 27525483]

Chaimayo C, Dunagan M, Hayashi T, Santoso N, and Takimoto T (2018). Specificity and functional interplay between influenza virus PA-X and NS1 shutoff activity. PLoS Pathog. 14, e1007465. [PubMed: 30496325]

Clark AM, Nogales A, Martinez-Sobrido L, Topham DJ, and DeDiego ML (2017). Functional Evolution of Influenza Virus NS1 Protein in Currently Circulating Human 2009 Pandemic H1N1 Viruses. J. Virol 91, e00721–17. [PubMed: 28637754]

Covarrubias S, Richner JM, Clyde K, Lee YJ, and Glaunsinger BA (2009). Host shutoff is a conserved phenotype of gammaherpesvirus infection and is orchestrated exclusively from the cytoplasm. J. Virol 83, 9554–9566. [PubMed: 19587049]

Covarrubias S, Gaglia MM, Kumar GR, Wong W, Jackson AO, and Glaunsinger BA (2011). Coordinated destruction of cellular messages in translation complexes by the gammaherpesvirus host shutoff factor and the mammalian exonuclease Xrn1. PLoS Pathog. 7, e1002339. [PubMed: 22046136]

Dadi S, Payet-Bornet D, and Ferrier P (2013). ImmunoPrecipitation of Nuclear Protein with Antibody Affinity Columns. Bio Protoc 3 10.21769/BioProtoc.319.

Das K, Ma L-C, Xiao R, Radvansky B, Aramini J, Zhao L, Marklund J, Kuo R-L, Twu KY, Arnold E, et al. (2008). Structural basis for suppression of a host antiviral response by influenza A virus. Proc. Natl. Acad. Sci. USA 105, 13093–13098. [PubMed: 18725644]

Dias A, Bouvier D, Crépin T, McCarthy AA, Hart DJ, Baudin F, Cusack S, and Ruigrok RWH (2009). The cap-snatching endonuclease of influenza virus polymerase resides in the PA subunit. Nature 458, 914–918. [PubMed: 19194459]

Doepker RC, Hsu W-L, Saffran HA, and Smiley JR (2004). Herpes simplex virus virion host shutoff protein is stimulated by translation initiation factors eIF4B and eIF4H. J. Virol 78, 4684–4699. [PubMed: 15078951]

Dubois J, Terrier O, and Rosa-Calatrava M (2014). Influenza viruses and mRNA splicing: doing more with less. MBio 5, e00070–14. [PubMed: 24825008]

Elgadi MM, Hayes CE, and Smiley JR (1999). The herpes simplex virus vhs protein induces endoribonucleolytic cleavage of target RNAs in cell extracts. J. Virol 73, 7153–7164. [PubMed: 10438802]

Esclatine A, Taddeo B, Evans L, and Roizman B (2004). The herpes simplex virus 1 UL41 gene-dependent destabilization of cellular RNAs is selective and may be sequence-specific. Proc. Natl. Acad. Sci. USA 101, 3603–3608. [PubMed: 14993598]

Feng P, Everly DN Jr., and Read GS (2001). mRNA decay during herpesvirus infections: interaction between a putative viral nuclease and a cellular translation factor. J. Virol 75, 10272–10280. [PubMed: 11581395]

Feng P, Everly DN Jr., and Read GS (2005). mRNA decay during herpes simplex virus (HSV) infections: protein-protein interactions involving the HSV virion host shutoff protein and translation factors eIF4H and eIF4A. J. Virol 79, 9651–9664. [PubMed: 16014927]

Feng F-L, Yu Y, Liu C, Zhang B-H, Cheng Q-B, Li B, Tan W-F, Luo X-J, and Jiang X-Q (2013). KAT5 silencing induces apoptosis of GBC-SD cells through p38MAPK-mediated upregulation of cleaved Casp9. Int. J. Clin. Exp. Pathol 7, 80–91. [PubMed: 24427328]

Firth AE, Jagger BW, Wise HM, Nelson CC, Parsawar K, Wills NM, Napthine S, Taubenberger JK, Digard P, and Atkins JF (2012). Ribosomal frameshifting used in influenza A virus expression occurs within the sequence UCC_UUU_CGU and is in the +1 direction. Open Biol. 2, 120109. [PubMed: 23155484]

Gaglia MM, Covarrubias S, Wong W, and Glaunsinger BA (2012). A common strategy for host RNA degradation by divergent viruses. J. Virol 86, 9527–9530. [PubMed: 22740404]

Gagnon KT, Li L, Janowski BA, and Corey DR (2014). Analysis of nuclear RNA interference in human cells by subcellular fractionation and Argonaute loading. Nat. Protoc 9, 2045–2060. [PubMed: 25079428]

Gao H, Sun Y, Hu J, Qi L, Wang J, Xiong X, Wang Y, He Q, Lin Y, Kong W, et al. (2015). The contribution of PA-X to the virulence of pandemic 2009 H1N1 and highly pathogenic H5N1 avian influenza viruses. Sci. Rep 5, 8262. [PubMed: 25652161]

Gasch AP, and Eisen MB (2002). Exploring the conditional coregulation of yeast gene expression through fuzzy k-means clustering. Genome Biol. 3, RESEARCH0059.

Glaunsinger B, and Ganem D (2004a). Lytic KSHV infection inhibits host gene expression by accelerating global mRNA turnover. Mol. Cell 13, 713–723. [PubMed: 15023341]

Glaunsinger B, and Ganem D (2004b). Highly selective escape from KSHV-mediated host mRNA shutoff and its implications for viral pathogenesis. J. Exp. Med 200, 391–398. [PubMed: 15289507]

Gong X-Q, Sun Y-F, Ruan B-Y, Liu X-M, Wang Q, Yang H-M, Wang S-Y, Zhang P, Wang X-H, Shan T-L, et al. (2017). PA-X protein decreases replication and pathogenicity of swine influenza virus in cultured cells and mouse models. Vet. Microbiol 205, 66–70. [PubMed: 28622865]

Gu B, Eick D, and Bensaude O (2013). CTD serine-2 plays a critical role in splicing and termination factor recruitment to RNA polymerase II in vivo. Nucleic Acids Res. 41, 1591–1603. [PubMed: 23275552]

Hale BG, Steel J, Medina RA, Manicassamy B, Ye J, Hickman D, Hai R, Schmolke M, Lowen AC, Perez DR, and García-Sastre A (2010). Inefficient control of host gene expression by the 2009 pandemic H1N1 influenza A virus NS1 protein. J. Virol 84, 6909–6922. [PubMed: 20444891]

Hardy JG, and Norbury CJ (2016). Cleavage factor Im (CFIm) as a regulator of alternative polyadenylation. Biochem. Soc. Trans 44, 1051–1057. [PubMed: 27528751]

Hayashi T, MacDonald LA, and Takimoto T (2015). Influenza A Virus Protein PA-X Contributes to Viral Growth and Suppression of the Host Antiviral and Immune Responses. J. Virol 89, 6442–6452. [PubMed: 25855745]

Hayashi T, Chaimayo C, McGuinness J, and Takimoto T (2016). Critical Role of the PA-X C-Terminal Domain of Influenza A Virus in Its Subcellular Localization and Shutoff Activity. J. Virol 90, 7131–7141. [PubMed: 27226377]

Heinz S, Texari L, Hayes MGB, Urbanowski M, Chang MW, Givarkes N, Rialdi A, White KM, Albrecht RA, Pache L, et al. (2018). Transcription Elongation Can Affect Genome 3D Structure. Cell 174, 1522–1536.e22. [PubMed: 30146161]

Hoffmann E, Neumann G, Kawaoka Y, Hobom G, and Webster RG (2000). A DNA transfection system for generation of influenza A virus from eight plasmids. Proc. Natl. Acad. Sci. USA 97, 6108–6113. [PubMed: 10801978]

Hsu J-L, Huang S-Y, Chow N-H, and Chen S-H (2003). Stable-isotope dimethyl labeling for quantitative proteomics. Anal. Chem 75, 6843–6852. [PubMed: 14670044]

Hu T, Zhang C, Tang Q, Su Y, Li B, Chen L, Zhang Z, Cai T, and Zhu Y (2013). Variant G6PD levels promote tumor cell proliferation or apoptosis via the STAT3/5 pathway in the human melanoma xenograft mouse model. BMC Cancer 13, 251. [PubMed: 23693134]

Hu J, Mo Y, Wang X, Gu M, Hu Z, Zhong L, Wu Q, Hao X, Hu S, Liu W, et al. (2015). PA-X decreases the pathogenicity of highly pathogenic H5N1 influenza A virus in avian species by inhibiting virus replication and host response. J. Virol 89, 4126–4142. [PubMed: 25631083]

Hu J, Mo Y, Gao Z, Wang X, Gu M, Liang Y, Cheng X, Hu S, Liu W, Liu H, et al. (2016). PA-X-associated early alleviation of the acute lung injury contributes to the attenuation of a highly pathogenic H5N1 avian influenza virus in mice. Med. Microbiol. Immunol 205, 381–395. [PubMed: 27289459]

Huang W, Sherman BT, and Lempicki RA (2009a). Bioinformatics enrichment tools: paths toward the comprehensive functional analysis of large gene lists. Nucleic Acids Res. 37, 1–13. [PubMed: 19033363]

Huang W, Sherman BT, and Lempicki RA (2009b). Systematic and integrative analysis of large gene lists using DAVID bioinformatics resources. Nat. Protoc 4, 44–57. [PubMed: 19131956]

Jagger BW, Wise HM, Kash JC, Walters K-A, Wills NM, Xiao Y-L, Dunfee RL, Schwartzman LM, Ozinsky A, Bell GL, et al. (2012). An over-lapping protein-coding region in influenza A virus segment 3 modulates the host response. Science 337, 199–204. [PubMed: 22745253]

Jewell NA, Cline T, Mertz SE, Smirnov SV, Flaño E, Schindler C, Grieves JL, Durbin RK, Kotenko SV, and Durbin JE (2010). Lambda interferon is the predominant interferon induced by influenza A virus infection in vivo. J. Virol 84, 11515–11522. [PubMed: 20739515]

Kamitani W, Narayanan K, Huang C, Lokugamage K, Ikegami T, Ito N, Kubo H, and Makino S (2006). Severe acute respiratory syndrome coronavirus nsp1 protein suppresses host gene expression by promoting host mRNA degradation. Proc. Natl. Acad. Sci. USA 103, 12885–12890. [PubMed: 16912115]

Kamitani W, Huang C, Narayanan K, Lokugamage KG, and Makino S (2009). A two-pronged strategy to suppress host protein synthesis by SARS coronavirus Nsp1 protein. Nat. Struct. Mol. Biol 16, 1134–1140. [PubMed: 19838190]

Khaperskyy DA, Hatchette TF, and McCormick C (2012). Influenza A virus inhibits cytoplasmic stress granule formation. FASEB J. 26, 1629–1639. [PubMed: 22202676]

Khaperskyy DA, Emara MM, Johnston BP, Anderson P, Hatchette TF, and McCormick C (2014). Influenza a virus host shutoff disables antiviral stress-induced translation arrest. PLoS Pathog. 10, e1004217. [PubMed: 25010204]

Khaperskyy DA, Schmaling S, Larkins-Ford J, McCormick C, and Gaglia MM (2016). Selective Degradation of Host RNA Polymerase II Transcripts by Influenza A Virus PA-X Host Shutoff Protein. PLoS Pathog. 12, e1005427. [PubMed: 26849127]

Kim S, Yamamoto J, Chen Y, Aida M, Wada T, Handa H, and Yamagu-chi Y (2010). Evidence that cleavage factor Im is a heterotetrameric protein complex controlling alternative polyadenylation. Genes Cells 15, 1003–1013. [PubMed: 20695905]

Kim D, Pertea G, Trapnell C, Pimentel H, Kelley R, and Salzberg SL (2013). TopHat2: accurate alignment of transcriptomes in the presence of insertions, deletions and gene fusions. Genome Biol. 14, R36. [PubMed: 23618408]

Kumar GR, and Glaunsinger BA (2010). Nuclear import of cytoplasmic poly(A) binding protein restricts gene expression via hyperadenylation and nuclear retention of mRNA. Mol. Cell. Biol 30, 4996–5008. [PubMed: 20823266]

Kumar GR, Shum L, and Glaunsinger BA (2011). Importin a-mediated nuclear import of cytoplasmic poly(A) binding protein occurs as a direct consequence of cytoplasmic mRNA depletion. Mol. Cell. Biol 31, 3113–3125. [PubMed: 21646427]

Lamb RA, and Choppin PW (1977). Synthesis of influenza virus polypeptides in cells resistant to alpha-amanitin: evidence for the involvement of cellular RNA polymerase II in virus replication. J. Virol 23, 816–819. [PubMed: 561196]

Lee YJ, and Glaunsinger BA (2009). Aberrant herpesvirus-induced polyadenylation correlates with cellular messenger RNA destruction. PLoS Biol. 7, e1000107. [PubMed: 19468299]

Li Q, Yuan X, Wang Q, Chang G, Wang F, Liu R, Zheng M, Chen G, Wen J, and Zhao G (2016). Interactomic landscape of PA-X-chicken protein complexes of H5N1 influenza A virus. J. Proteomics 148, 20–25. [PubMed: 27422376]

Martinson HG (2011). An active role for splicing in 3′-end formation. Wiley Interdiscip. Rev. RNA 2, 459–470. [PubMed: 21957037]

Matrosovich M, Matrosovich T, Garten W, and Klenk H-D (2006). New low-viscosity overlay medium for viral plaque assays. Virol. J 3, 63. [PubMed: 16945126]

Morgado A, Almeida F, Teixeira A, Silva AL, and Romão L (2012). Unspliced precursors of NMD-sensitive β-globin transcripts exhibit decreased steady-state levels in erythroid cells. PLoS One 7, e38505. [PubMed: 22675570]

Muller M, and Glaunsinger BA (2017). Nuclease escape elements protect messenger RNA against cleavage by multiple viral endonucleases. PLoS Pathog. 13, e1006593. [PubMed: 28841715]

Muller M, Hutin S, Marigold O, Li KH, Burlingame A, and Glaunsinger BA (2015). A ribonucleoprotein complex protects the interleukin-6 mRNA from degradation by distinct herpesviral endonucleases. PLoS Pathog. 11, e1004899. [PubMed: 25965334]

Nemeroff ME, Barabino SM, Li Y, Keller W, and Krug RM (1998). Influenza virus NS1 protein interacts with the cellular 30 kDa subunit of CPSF and inhibits 3′ end formation of cellular pre-mRNAs. Mol. Cell 1, 991–1000. [PubMed: 9651582]

Nogales A, Martinez-Sobrido L, Chiem K, Topham DJ, and DeDiego ML (2018). Functional Evolution of the 2009 Pandemic H1N1 Influenza Virus NS1 and PA in Humans. J. Virol 92, e01206–18. [PubMed: 30021892]

Oishi K, Yamayoshi S, and Kawaoka Y (2015). Mapping of a Region of the PA-X Protein of Influenza A Virus That Is Important for Its Shutoff Activity. J. Virol 89, 8661–8665. [PubMed: 26041295]

Rappsilber J, Ryder U, Lamond AI, and Mann M (2002). Large-scale proteomic analysis of the human spliceosome. Genome Res. 12, 1231–1245. [PubMed: 12176931]

Rodriguez A, Pérez-González A, Hossain MJ, Chen L-M, Rolling T, Pérez-Breña P, Donis R, Kochs G, and Nieto A (2009). Attenuated strains of influenza A viruses do not induce degradation of RNA polymerase II. J. Virol 83, 11166–11174. [PubMed: 19692472]

Roux KJ, Kim DI, Raida M, and Burke B (2012). A promiscuous biotin ligase fusion protein identifies proximal and interacting proteins in mammalian cells. J. Cell Biol. 196, 801–810. [PubMed: 22412018]

Rowe M, Glaunsinger B, van Leeuwen D, Zuo J, Sweetman D, Ganem D, Middeldorp J, Wiertz EJHJ, and Ressing ME (2007). Host shutoff during productive Epstein-Barr virus infection is mediated by BGLF5 and may contribute to immune evasion. Proc. Natl. Acad. Sci. USA 104, 3366–3371. [PubMed: 17360652]

Sadek J, and Read GS (2016). The Splicing History of an mRNA Affects Its Level of Translation and Sensitivity to Cleavage by the Virion Host Shutoff Endonuclease during Herpes Simplex Virus Infections. J. Virol 90, 10844–10856. [PubMed: 27681125]

Salvatore M, Basler CF, Parisien J-P, Horvath CM, Bourmakina S, Zheng H, Muster T, Palese P, and García-Sastre A (2002). Effects of influenza A virus NS1 protein on protein expression: the NS1 protein enhances translation and is not required for shutoff of host protein synthesis. J. Virol 76, 1206–1212. [PubMed: 11773396]

Schoggins JW, Wilson SJ, Panis M, Murphy MY, Jones CT, Bieniasz P, and Rice CM (2011). A diverse range of gene products are effectors of the type I interferon antiviral response. Nature 472, 481–485. [PubMed: 21478870]

Shi M, Jagger BW, Wise HM, Digard P, Holmes EC, and Taubenberger JK (2012). Evolutionary conservation of the PA-X open reading frame in segment 3 of influenza A virus. J. Virol 86, 12411–12413. [PubMed: 22951836]

Singh G, Rebbapragada I, and Lykke-Andersen J (2008). A competition between stimulators and antagonists of Upf complex recruitment governs human nonsense-mediated mRNA decay. PLoS Biol. 6, e111. [PubMed: 18447585]

Slaine PD, MacRae C, Kleer M, Lamoureux E, McAlpine S, Warhuus M, Comeau AM, McCormick C, Hatchette T, and Khaperskyy DA (2018). Adaptive Mutations in Influenza A/California/07/2009 Enhance Polymerase Activity and Infectious Virion Production. Viruses 10, 272.

Szklarczyk D, Morris JH, Cook H, Kuhn M, Wyder S, Simonovic M, Santos A, Doncheva NT, Roth A, Bork P, et al. (2017). The STRING database in 2017: quality-controlled protein-protein association networks, made broadly accessible. Nucleic Acids Res. 45 (D1), D362–D368. [PubMed: 27924014]

Trapnell C, Roberts A, Goff L, Pertea G, Kim D, Kelley DR, Pimentel H, Salzberg SL, Rinn JL, and Pachter L (2012). Differential gene and transcript expression analysis of RNA-seq experiments with TopHat and Cufflinks. Nat. Protoc 7, 562–578. [PubMed: 22383036]

Wang X, Spandidos A, Wang H, and Seed B (2012). PrimerBank: a PCR primer database for quantitative gene expression analysis, 2012 update. Nucleic Acids Res. 40, D1144–D1149. [PubMed: 22086960]

Xu G, Zhang X, Liu Q, Bing G, Hu Z, Sun H, Xiong X, Jiang M, He Q, Wang Y, et al. (2017). PA-X protein contributes to virulence of triple-reassortant H1N2 influenza virus by suppressing early immune responses in swine. Virology 508, 45–53. [PubMed: 28494344]

Yeo G, and Burge CB (2004). Maximum entropy modeling of short sequence motifs with applications to RNA splicing signals. J. Comput. Biol 11, 377–394. [PubMed: 15285897]

Younis I, Berg M, Kaida D, Dittmar K, Wang C, and Dreyfuss G (2010). Rapid-response splicing reporter screens identify differential regulators of constitutive and alternative splicing. Mol. Cell. Biol 30, 1718–1728. [PubMed: 20123975]

Yuan P, Bartlam M, Lou Z, Chen S, Zhou J, He X, Lv Z, Ge R, Li X, Deng T, et al. (2009). Crystal structure of an avian influenza polymerase PA(N) reveals an endonuclease active site. Nature 458, 909–913. [PubMed: 19194458]

Zhao N, Sebastiano V, Moshkina N, Mena N, Hultquist J, Jimenez-Morales D, Ma Y, Rialdi A, Albrecht R, Fenouil R, et al. (2018). Influenza virus infection causes global RNAPII termination defects. Nat. Struct. Mol. Biol 25, 885–893. [PubMed: 30177761]

Zhou Z, Licklider LJ, Gygi SP, and Reed R (2002). Comprehensive proteomic analysis of the human spliceosome. Nature 419, 182–185. [PubMed: 12226669]

Zhu Y, Wang X, Forouzmand E, Jeong J, Qiao F, Sowd GA, Engelman AN, Xie X, Hertel KJ, and Shi Y (2018). Molecular Mechanisms for CFIm-Mediated Regulation of mRNA Alternative Polyadenylation. Mol. Cell 69, 62–74.e4. [PubMed: 29276085]

Highlights

- Influenza A virus PA-X targets the majority of host mRNAs for destruction
- Downregulation by PA-X correlates with the number of splice sites in a transcript
- Splicing renders RNAs susceptible to PA-X
- The cellular CFIm complex interacts with PA-X and contributes to PA-X activity

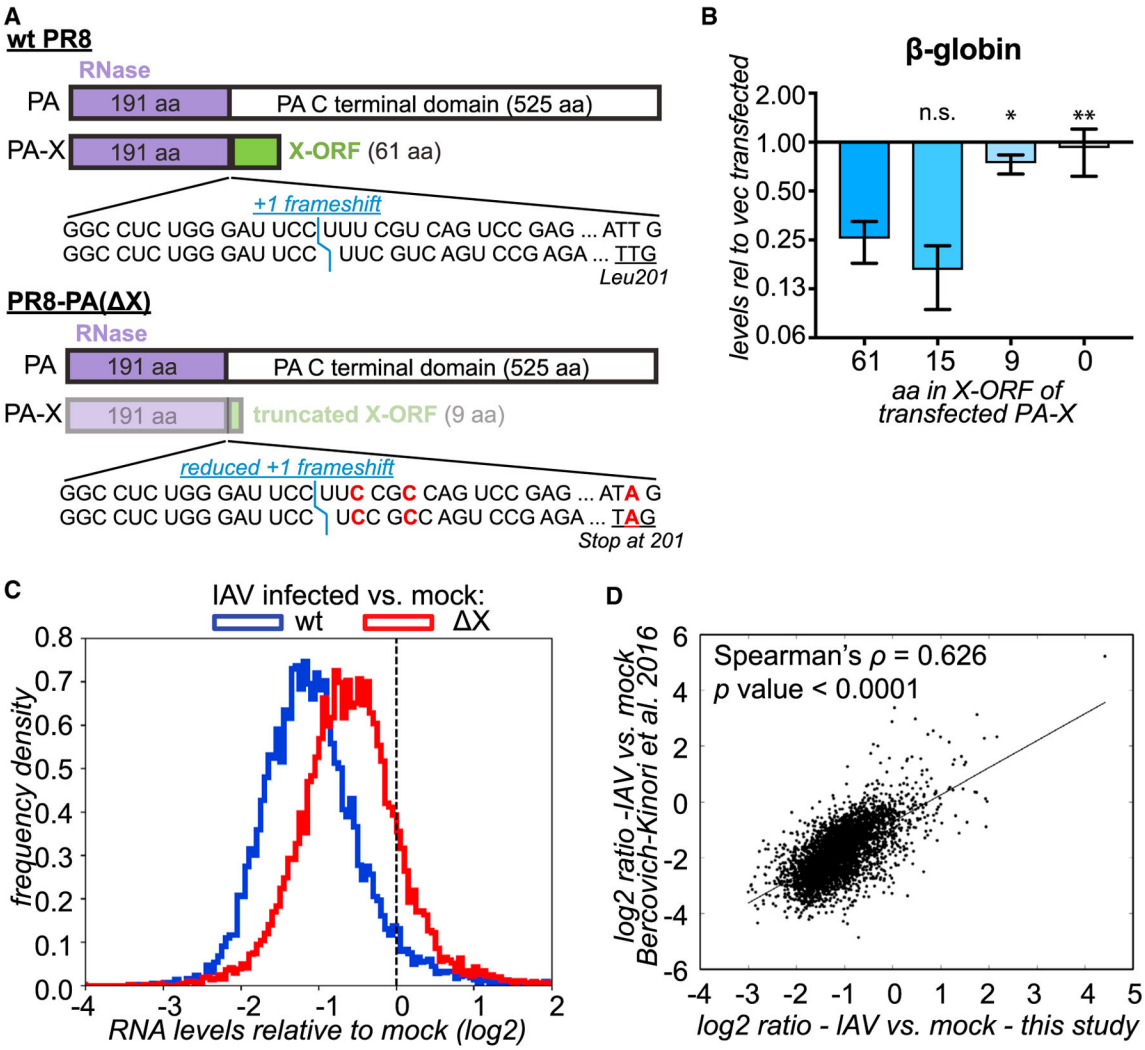

Figure 1. PA-X Downregulates Most Cellular RNAs and Is a Major Contributor to Host Shutoff during Influenza A Virus Infection

(A) Diagram of mutations in the PR8 PA(ΔX) virus. Less intense colors indicate lower levels of PA-X. Blue, position of the frameshift. Red, mutated nucleotides in the frameshifting sequence and at PA-X codon 201.

(B) HEK293T cells were transfected for 24 h with a β-globin reporter and WT PR8 PA-X ("61") or variants with the C-terminal X-ORF truncated after the indicated number of amino acids (aa). Levels of β-globin in PA-X transfected cells were measured by RT-qPCR and are plotted relative to vector transfected cells, after normalization to cellular 18S rRNA. Values represent means ± SDs. n = 3. *p < 0.05, and **p< 0.01, ANOVA followed by Dunnett's multiple comparison test versus WT PA-X (61 aa).

(C) RNA-seq was carried out on RNA collected 15 h after infection from A549 cells infected with WT PR8 or PR8 PA(ΔX). The ratio between levels in IAV-infected versus mock-infected cells was computed for each RNA and the distribution of the ratios (log2) is plotted as a frequency histogram. The populations are significantly different (p < 0.001)

based on the Kolmogorov-Smirnoff test. The dashed line indicated a ratio of 1 (no change). $n \geq 2$.

(D) The ratio in RNA levels in WT IAV-infected cells versus mock-infected cells in our study (15 h post-infection, MOI = 1) is plotted against the results from Bercovich-Kinori et al. (2016) (8 h post-infection, MOI = 5). $p < 0.001$, Spearman's test.

See also Figures S1 and S2.

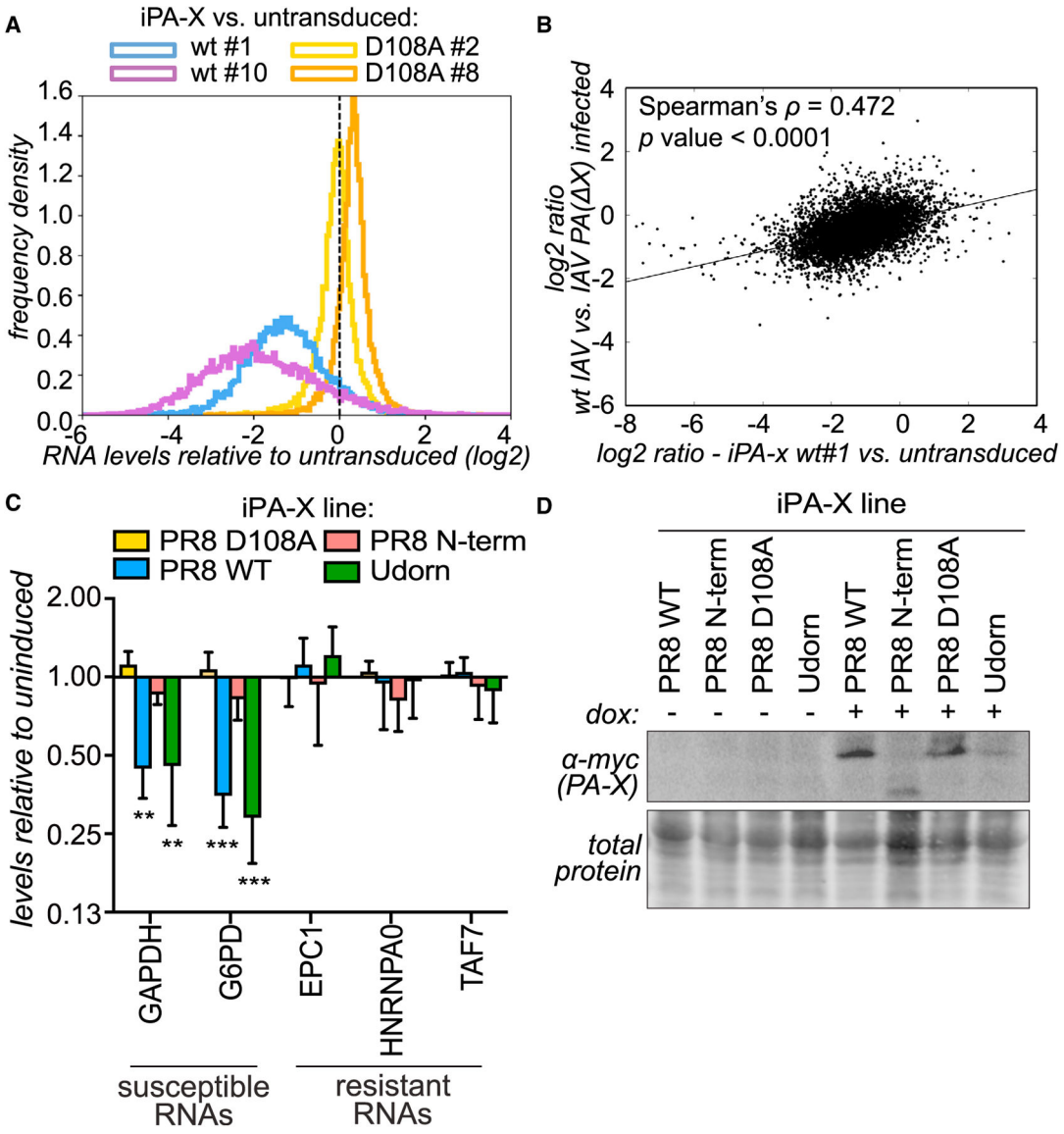

Figure 2. PA-X Downregulates Most Cellular RNAs in the Absence of Other Viral Proteins

RNA and protein samples were collected from control (untransduced) A549 cells or A549 cells expressing doxycycline-inducible PR8 PA-X (WT), PR8 PA-X catalytic mutant (D108A), PR8 PA-X N-terminal endonuclease domain (aa 1–191, "N term"), or Udorn PA-X 18 h after the addition of doxycycline.

(A) RNA-seq was carried out on cells expressing WT or mutant PR8 PA-X (2 clonal lines for each). The ratio between the levels in PA-X-expressing versus control cells was computed for each RNA, and the distribution of the ratios is plotted as a frequency histogram. The dashed line indicates a ratio of 1 (no change). $n \geq 2$.

(B) The PA-X-dependent changes in RNA levels in infected cells (ratio in PR8 PA(ΔX) versus WT PR8) are plotted against changes in cells expressing PR8 PA-X versus control cells. $p < 0.001$, Spearman's test.

(C) Levels of several endogenous mRNAs were measured by RT-qPCR in cells expressing the indicated PA-X variants. After normalization to 18S, mRNA levels are plotted relative to uninduced cells. Values represent means ± SDs. $n \geq 3$. **$p < 0.01$ and ***$p < 0.001$. ANOVA followed by Dunnett's multiple comparison test versus PR8 PA-X D108A.
(D) A representative western blot using anti-myc antibodies to detect myc-tagged PA-X and a total protein stain as loading control (blot section from 25 to 35 kDa) shows successful induction of PA-X in each cell line (corresponds to one of the experiments shown in C).

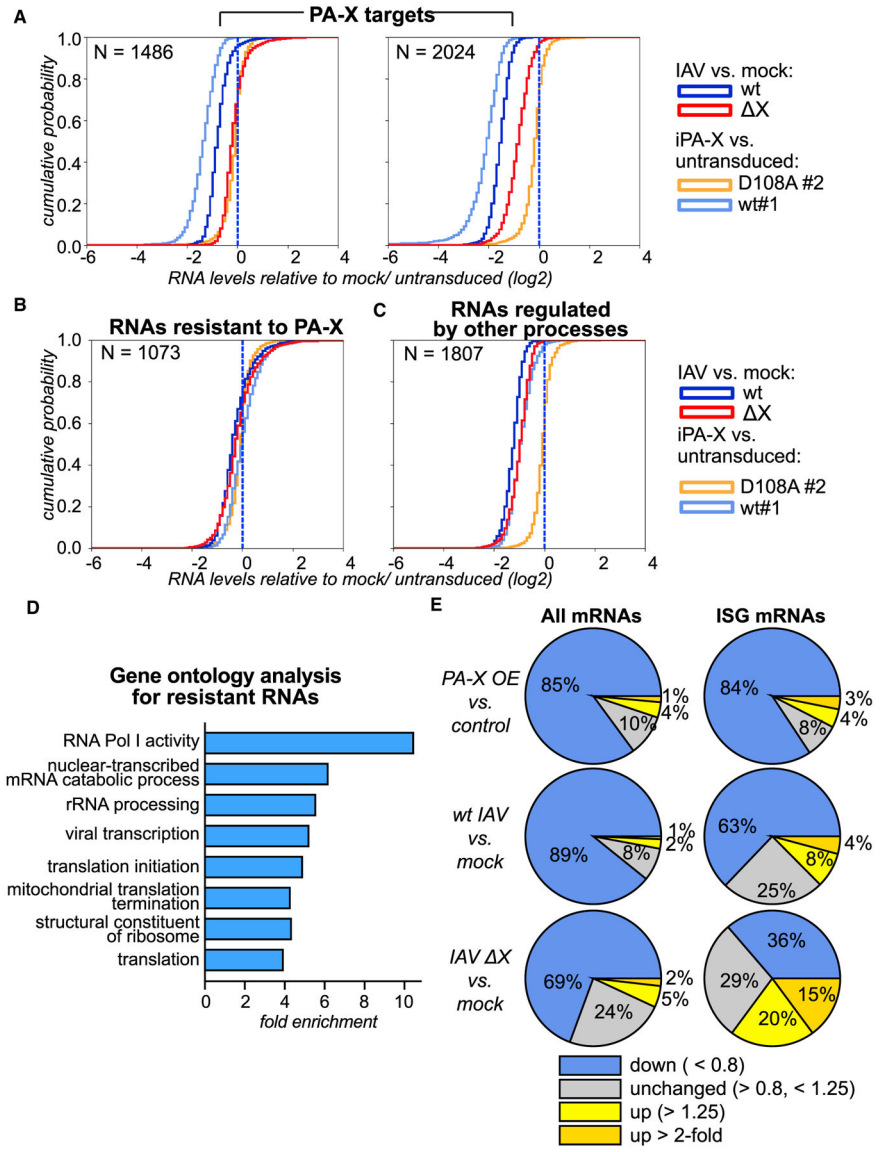

Figure 3. k-Means Clustering Reveals Differentially Regulated Groups of RNAs

(A–C) Cluster 3 was used to divide cellular RNAs in 4 clusters based on the pattern of fold changes in iPA-X cells (PA-X WT or D108A catalytic mutant versus control) and cells infected with IAV (WT or PA-X-deficient IAV versus mock). Cumulative probability histograms of fold changes for each of the classes are plotted: (A) 2 groups of PA-X targets, (B) PA-X-resistant RNAs, (C) potential PA-X targets that are regulated by other processes during infection. All of the datasets collected were used for clustering, but only select datasets are plotted for simplicity.

(D) DAVID was used to identify overrepresented Gene Ontology (GO) terms for biological processes and molecular functions among PA-X-resistant RNAs. Fold enrichment is plotted for GO terms that had corrected $p < 0.01$.

(E) Pie charts showing the percentage of genes that are up- and downregulated in infected and iPA-X cells. Left: all RNAs detected in RNA-seq (WT versus mock: N = 8,573, PR8

PA(ΔX) versus mock: N = 8,848, PA-X overexpression (OE) versus control: N = 8,554). Right: interferon-stimulated genes (ISGs; WT versus mock: N = 167, PR8 PA(ΔX) versus mock: N = 168, PA-X OE versus control: N = 159).

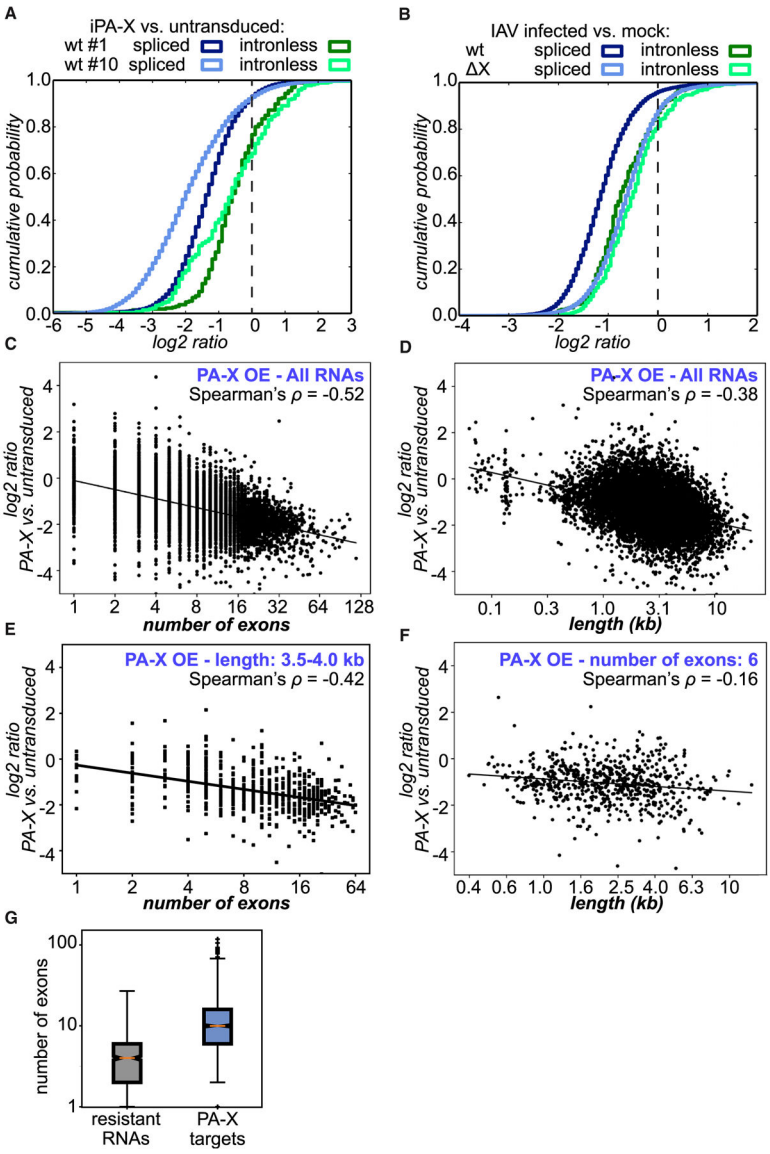

Figure 4. RNAs that Are Not Spliced Are Less Sensitive to Regulation by PA-X

(A and B) RNA-seq results from Figures 1C and 2A are plotted separately for spliced and intronless RNA as cumulative distribution histograms. (A) Cells overexpressing WT PA-X, clones #1 and #10; (B) cells infected with WT PR8 versus PR8 PA(ΔX).

(C–F) Relative RNA levels in PA-X overexpressing (OE; clone #1) versus control cells are plotted against the number of exons (C and E, log2 scale) or transcript length in kilobases (D and F, log10 scale). (C and D) All RNAs, (E) RNAs with 6 exons, and (F) RNAs 3.5–4.0 kb in length. All of the correlations are statistically significant ($p < 0.001$, Spearman's test).

(G) The number of exons for RNAs identified in the clustering analysis (Figure 3) is plotted. The two groups of PA-X targets (Figure 3A) are plotted together. $p < 0.01$, Kolmogorov-Smirnoff test.

See also Figure S3.

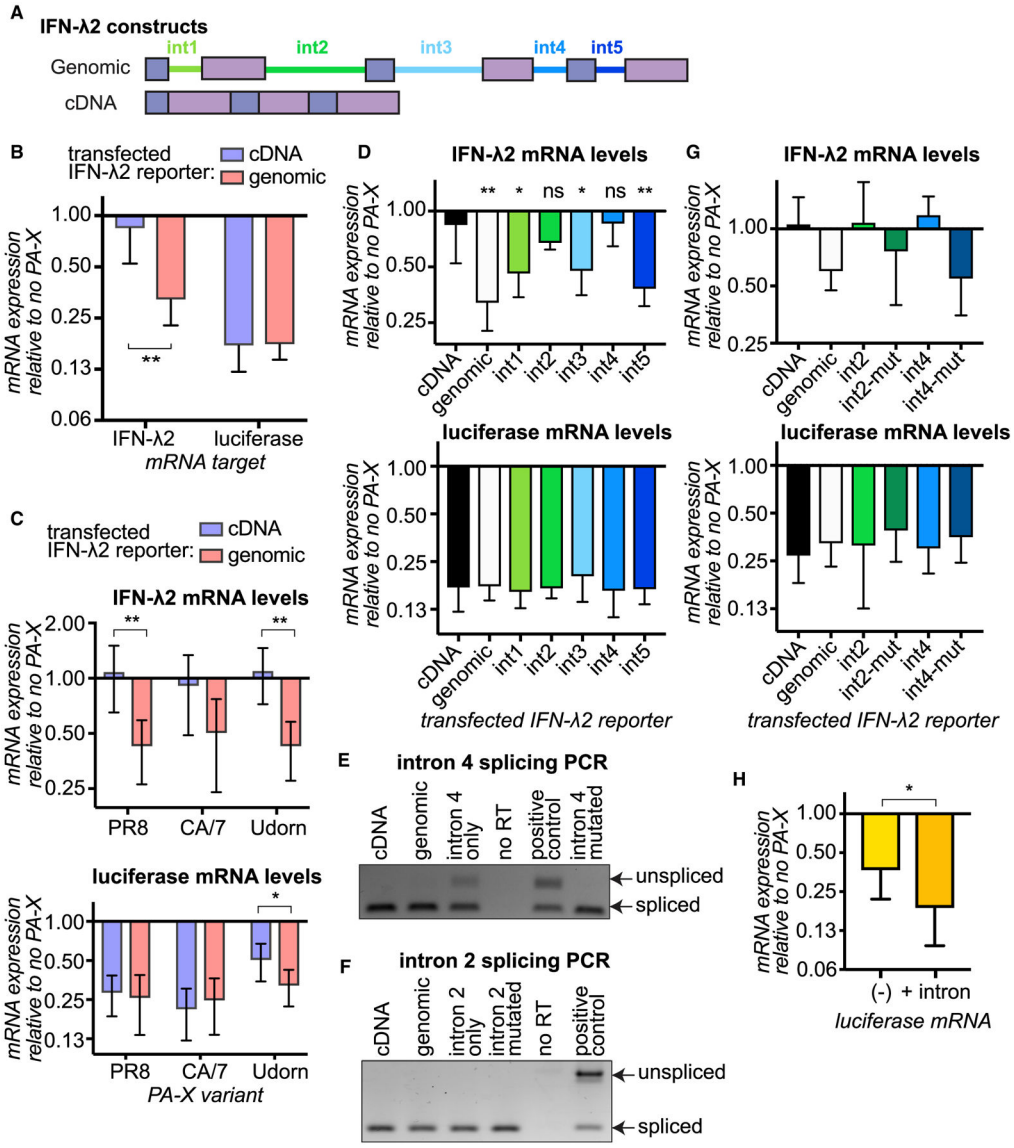

Figure 5. Addition of Introns and Splicing Events Promotes Degradation by PA-X

(A) Diagram of IFN-λ2 constructs. Int, intron.

(B–G) HEK293T cells were transfected for 24 h, with reporters expressing a luciferase control mRNA and IFN-λ2 mRNA from cDNA, the genomic locus, cDNA with 1 of the 5 IFN-λ2 introns added back, or cDNA with IFN-λ2 introns 2 or 4 carrying mutations that restore a canonical 5′ splice site sequence. Cells were also transfected with PA-X (PR8 variant in B, D, and G; PR8, CA/7, and Udorn variants in C) or vector. Levels of luciferase and IFN-λ2 mRNAs were measured by RT-qPCR and plotted as relative levels in PA-X expressing versus vector-transfected cells, after normalization to 18S rRNA. The downregulation of a spliced luciferase mRNA serves as a control to ensure similar PA-X activity across samples. In (E) and (F), cDNA from vector-transfected cells was PCR amplified across the indicated introns to test splicing. Amplified PCR products are shown (image is representative of 4 experiments). A 1:1 mix of the IFN-λ2 cDNA and genomic

constructs was included to check that unspliced and spliced products could be simultaneously amplified.

(H) Cells were transfected with an intronless (−) or an intron-containing (+ intron) luciferase reporter and PR8 PA-X. Luciferase RNA levels were measured by RT-qPCR, normalized by 18S rRNA, and were plotted relative to vector-transfected cells.

Values represent means ± SDs; $n \geq 4$. *$p < 0.05$, **$p < 0.01$; For (B) and (C), ANOVA followed by Tukey's pairwise test; (D) ANOVA followed by Dunnett's test, p values relative to cDNA construct; (H) Student's t test. See also Figure S4.

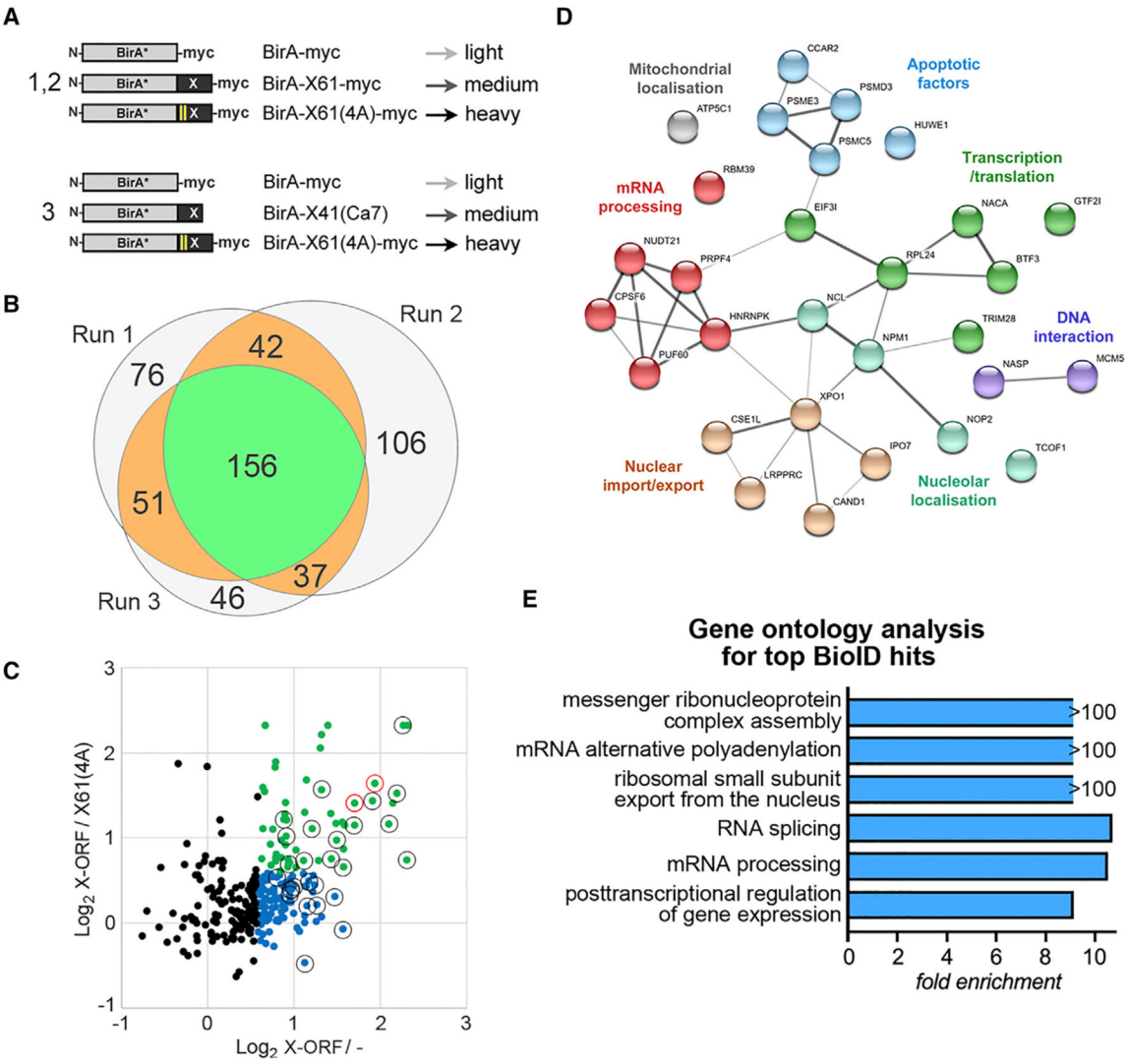

Figure 6. The X-ORF Interactome Is Enriched for Proteins Involved in mRNA Processing

(A) Schematic diagram of X-ORF-BirA* fusion baits used in the BioID mass spectrometry experiment. The numbers indicate independent runs using each construct set. Light, medium, and heavy = light, medium, or heavy isotope tags.

(B) Overlap between proteins identified by mass spectrometry by ≥2 unique peptides in 3 BioID runs.

(C) Average relative abundance of 286 proteins identified in at least 2 BioID experiments, plotted as log2 ratio of medium versus light (x axis, X-ORF/−) and medium versus heavy (y axis, X-ORF/X61(4A)). Green dots represent proteins with >1.5-fold enrichment over both negative controls; blue dots represent proteins with >1.5-fold enrichment over BirA*-myc alone; black and red open circles represent high-confidence hits (>2.0-fold over BirA*-myc in ≥2 experiments or >1.5-fold over BirA*-myc and BirA*-X61(4A)-myc in 3 experiments); red open circles represent nucleolin (NCL) and nucleophosmin (NPM1), which were enriched >2.0-fold over both negative controls in all 3 experiments.

(D) STRING protein-protein interaction network of high-confidence hits. Apparent nodes were differentially colored (only 1 annotation per protein is shown for simplicity).
(E) Gene Ontology (GO) enrichment analysis of X-ORF BioID hits (black and red circles in C). All enriched functional classes are presented (excluding parental subclasses for each term). Note that the >100-fold enriched functional classes contain only 2 proteins each.
See also Figure S5.

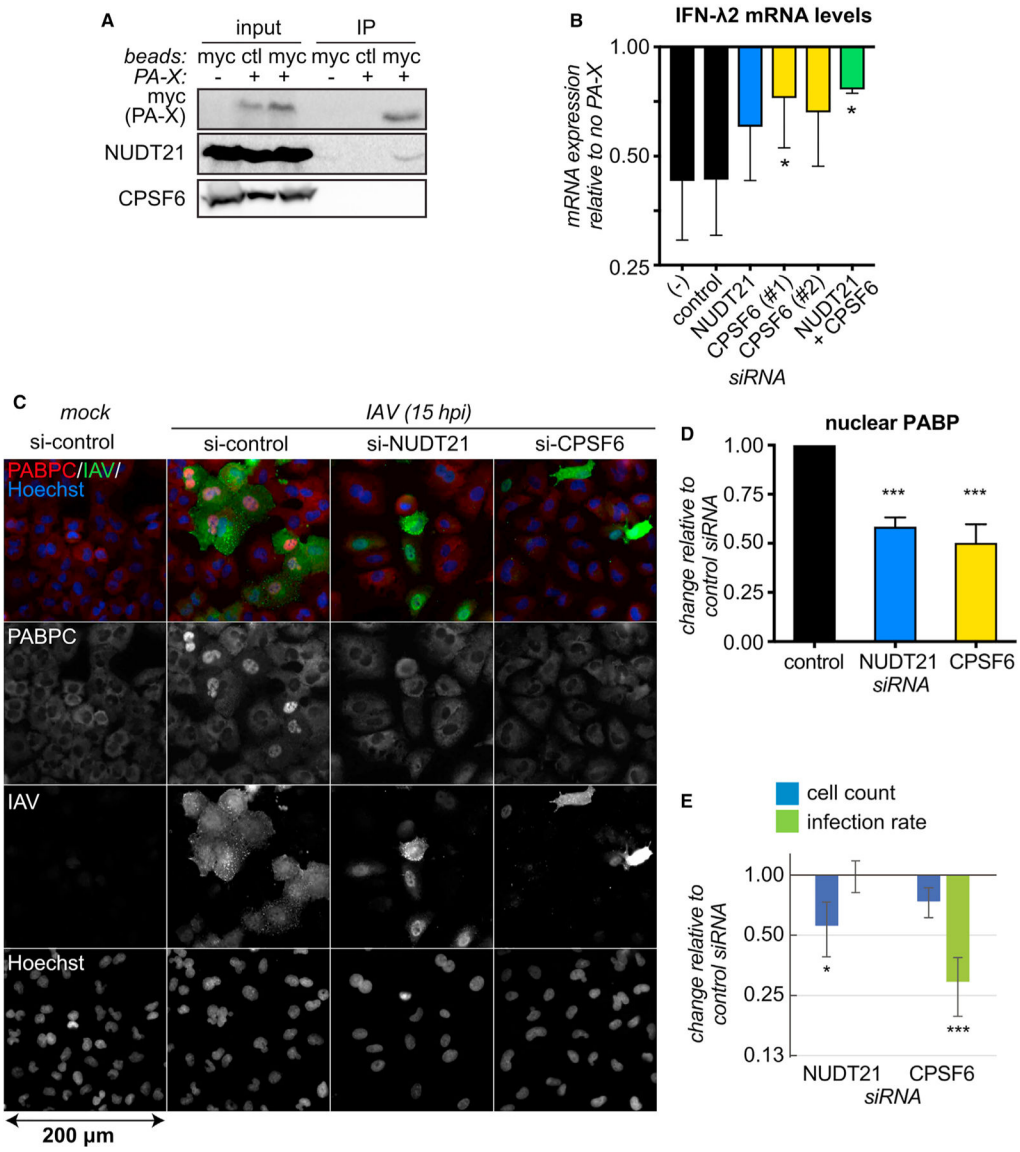

Figure 7. The CFIm Complex Is Involved in PA-X Activity

(A) Proteins were extracted from the nuclei of uninduced or doxycycline-treated HEK293T cells expressing inducible WT PR8 PA-X, and incubated with myc-trap beads to immunoprecipitate PA-X-myc (myc) or control beads (ctrl). Input and immunoprecipitation (IP) samples were resolved by SDS-PAGE and analyzed by western blotting for PA-X-myc, NUDT21, and CPSF6. The image is representative of 3 independent experiments.

(B) NUDT21 and CPSF6 were knocked down by siRNA, separately or in combination, in HEK293T cells. For NUDT21, siRNA #2 was used (see STAR Methods). For CPSF6, siRNA #1 was used for knockdown in combination with NUDT21. Cells were then transfected with a reporter expressing IFN-λ2 mRNA from the genomic locus, with and without WT PR8 PA-X. The levels of IFN-λ2 mRNA and 18S rRNA were measured by RT-qPCR. The expression of IFN-λ2 mRNA is plotted relative to vector-transfected cells, after normalization to 18S rRNA.

(C–E) NUDT21 and CPSF6 were knocked down by siRNA in A549 cells, using a mixture of 2 siRNAs. Cells were then infected with WT PR8 IAV for 15 h. Infection rates were assessed by staining for IAV proteins and host shutoff by staining for nuclear PABP.
(C) Representative immunofluorescence images. Scale bar, 200 μm, indicated as an arrow in the lower left corner.
(D and E) change in the fraction of infected cells with nuclear PABP (D) or total cell counts and infected cells (E), relative to control siRNA. Bars are means ± SDs; $n \geq 3$. *$p < 0.05$ and ***$p < 0.001$. ANOVA followed by Dunnett's multiple comparison test versus control siRNA. See also Figure S6.

KEY RESOURCES TABLE

REAGENT or RESOURCE	SOURCE	IDENTIFIER
Antibodies		
CPSF6 (clone F-3)	Santa Cruz Biotechnology	Cat#sc-376228; RRID: AB_10992032
NUDT21 (clone 2203C3)	Santa Cruz Biotechnology	Cat#sc-81109; RRID: AB_2153989
PABPC1 (clone 10E10)	Santa Cruz Biotechnology	Cat#sc-32318; RRID: AB_628097
Tubulin (clone H-235)	Santa Cruz Biotechnology	Cat#sc-9104; RRID: AB_2241191
Myctag (clone 9B11)	Cell Signaling Technologies	Cat#2276; RRID: AB_331783
Nucleophosmin	Cell Signaling Technologies	Cat#3542; RRID: AB_2155178
Influenza A virus	Abeam	Cat#ab20841; RRID: AB_775660
Nucleolin	Abeam	Cat#ab22758; RRID: AB_776878
Firefly luciferase	Abeam	Cat#ab21176; RRID: AB_446076
IFNL2/IL-28A	Abeam	Cat#ab109820; RRID: AB_10859066
PUF60	Bethyl Laboratories	Cat#A302-817A; RRID: ABJ0631036
RBM39	Atlas	Cat#HPA001591; RRID: AB_1079749
Anti-mouse secondary coupled to horseradish peroxidase	Southern Biotech	Cat#103005; RRID: AB_2619742
Anti-rabbit secondary coupled to horseradish peroxidase	Southern Biotech	Cat#403005; RRID: AB_2687483
Anti-goat secondary coupled to horseradish peroxidase	Southern Biotech	Cat#616005
Anti-goat secondary coupled to Alexa Fluor-488	Thermo Fisher	Cat # A-11055; RRID: AB_2534102
Anti-mouse secondary coupled to Alexa Fluor-555	Thermo Fisher	Cat # A-31570; RRID: AB_2536180
Bacterial and Virus Strains		
Influenza A virus A/Puerto Rico/8/34 H1N1	Khaperskyy et al., 2012	PR8
Influenza A virus A/Puerto Rico/8/34 H1N1 PA(fs)	Khaperskyy et al., 2016	PR8 PA(fs)
Influenza A virus A/Puerto Rico/8/34 H1N1 PA(X9)	This paper	PR8 PA(X9)
Influenza A virus A/Puerto Rico/8/34 H1N1 PA(AX)	This paper	PR8 PA(ΔX)
Chemicals, Peptides, and Recombinant Proteins		
Streptavidin conjugated to Alexa Fluor-488	Life Technologies / Thermo Fisher / Molecular Probes	Cat # S32354; RRID: AB_2315383
Streptavidin conjugated to horseradish peroxidase	Cell Signaling Technologies	Cat # 3999; RRID:AB_10830897
Lipofectamine RNAiMAX transfection reagent	Life Technologies / Thermo Fisher	Cat # 13778150
Trizol	Life Technologies / Thermo Fisher	Cat # 15596018
Turbo DNase	Life Technologies / Thermo Fisher	Cat # AM2239
RNase A	QIAGEN	Cat # 19101
HiFi assembly mix	New England Biolabs	E5520S
polyethylenimine	VWR	Cat # 87001–912
Doxycycline	Fisher	BP26531
MycTrap magnetic agarose beads	ChromoTek	Cat# ymta-20; RRID: AB_2631370
Control magnetic agarose beads	ChromoTek	Cat# bmab-20
complete protease inhibitors	Roche	Cat# 11873580001
Total protein stain for Li-Cor	LI-COR biosciences	P/N926–11010
Critical Commercial Assays		
iScript Reverse Transcription Supermix for RT-qPCR	Bio-Rad	170–8841

REAGENT or RESOURCE	SOURCE	IDENTIFIER
Quick-RNA miniprep kit	Zymo Research	R1050
iTaq Universal SYBR® Green Supermix	Bio-Rad	172–5125
RNeasy Plus minikit	QIAGEN	74134
ERCC ExFold RNA spike-in mix	Life Technologies / Thermo Fisher	4456739
TruSeq Stranded Total RNA Library Prep Kit with Ribo-Zero Human	Illumina	RS-122–2301
High Capacity Neutravidin Agarose Beads	Thermo Fisher	Cat # 29200
Pierce Trypsin protease, MS-Grade	Thermo Fisher	Cat # 90057
Deposited Data		
Raw sequencing data and fold changes	This paper, GEO (NCBI)	GEO:GSE120183
Experimental Models: Cell Lines		
Human epithelial kidney cells HEK293A	Thermo Fisher	Cat # R70507
Human epithelial kidney cells HEK293T	ATCC	ATCCCRL-3216
Human adenocarcinoma alveolar basal epithelial cells A549	ATCC	ATCCCCL-185
Human adenocarcinoma alveolar basal epithelial cells A549 - inducible PR8 PA-X wt line #1	Khaperskyy et al., 2016	A549 iPA-X wt #1
Human adenocarcinoma alveolar basal epithelial cells A549 - inducible PR8 PA-X wt line #10	Khaperskyy et al., 2016	A549iPA-X wt #10
Human adenocarcinoma alveolar basal epithelial cells A549 - inducible PR8 PA-X D108A line #2	Khaperskyy et al., 2016	A549iPA-XD108A #2
Human adenocarcinoma alveolar basal epithelial cells A549 - inducible PR8 PA-X D108A line #8	Khaperskyy et al., 2016	A549iPA-XD108A #8
Human adenocarcinoma alveolar basal epithelial cells A549 - inducible Udorn PA-X wt line #18	This paper	A549 iPA-X Udorn
Human adenocarcinoma alveolar basal epithelial cells A549 - inducible PR8 PA-X N terminus (aa 1–191) line #8	This paper	A549 iPA-X Nterm
Human epithelial kidney cells HEK293T inducible PR8 PA-X wt line #T7	Khaperskyy et al., 2016	293T iPA-X wt
Oligonucleotides		
Control Stealth siRNA	Life Technologies / Thermo Fisher	Cat #12935300
NUDT21 Stealth siRNA (#1)	Life Technologies / Thermo Fisher	Cat # 1299001 - HSS117100
NUDT21 Stealth siRNA (#2) (used for Figure 7B)	Life Technologies / Thermo Fisher	Cat #1299001 - HSS117102
CPSF6 Stealth siRNA (#1)	Life Technologies / Thermo Fisher	Cat #1299001 - HSS117104
CPSF6 Stealth siRNA (#2)	Life Technologies / Thermo Fisher	Cat # 1299001 - HSS117103
Nucleolin Stealth siRNA	Life Technologies / Thermo Fisher	Cat # 1299001 - HSS106985
Nucleolin Stealth siRNA	Life Technologies / Thermo Fisher	Cat # 1299001 - HSS106984
RBM39 Stealth siRNA	Life Technologies / Thermo Fisher	Cat #1299001 - HSS145210
RBM39 Stealth siRNA	Life Technologies / Thermo Fisher	Cat # 1299001 - HSS145212
Primers for qPCR and splicing assays	This paper	See Table S3
Recombinant DNA		
pCR3.1-PA-X_PR8-myc	Khaperskyy et al., 2014	N/A
pCR3.1-PA-X_TN/CA/7-myc	Khaperskyy et al., 2016	N/A
pCR3.1-PA-N191_PR8-myc	Khaperskyy et al., 2016	N/A
pCR3.1-PA-X_Udorn-myc	This paper	N/A

REAGENT or RESOURCE	SOURCE	IDENTIFIER
pCR3.1-PA-X_15aa_PR8-myc	This paper	N/A
pCR3.1-PA-X_9aa_PR8-myc	This paper	N/A
pTRIPZ_PA-X-Nterm (aa 1–191)_ PR8-myc	This paper	N/A
pTRIPZ_PA-X_Udom-myc	This paper	N/A
pCMV-IFNL2 cDNA	This paper	N/A
pCMV-IFNL2 genomic	This paper	N/A
pCMV-IFNL2 intron 1 only	This paper	N/A
pCMV-IFNL2 intron 2 only	This paper	N/A
pCMV-IFNL2 intron 3 only	This paper	N/A
pCMV-IFNL2 intron 4 only	This paper	N/A
pCMV-IFNL2 intron 5 only	This paper	N/A
pCMV-IFNL2 mutated intron 2 only	This paper	N/A
pCMV-IFNL2 mutated intron 4 only	This paper	N/A
pcDNA3.1-myc-BiolD2-MCS	Roux et al., 2012	Addgene # 74223
pCR3.1-BirA*-myc	This paper	N/A
pCR3.1-BirA*-X61-myc	This paper	N/A
pCR3.1-BirA*-X61 (4A)-myc	This paper	N/A
pCR3.1-BirA*-X41(CA/7)	This paper	N/A
CMV-LUC2CP/intron/ARE	Gift from Gideon Dreyfuss; Younis et al., 2010	N/A
CMV-LUC2CP/ARE	Gift from Gideon Dreyfuss; Younis et al., 2010	N/A
pCDNA3.1-p-globin	Covarrubias et al., 2011	N/A
Software and Algorithms		
Prism 7	GraphPad	N/A
Tophat	Kim et al., 2013, https://ccb.jhu.edu/software/tophat/index.shtml	V2.1.1
Cufflinks	Trapnell et al., 2012, http://cole-trapnell-lab.github.io/cufflinks/	V2.2.1
GeneSys (chemiblot imager)	Syngene	V1.5.4.0
Image Studio 5.2 (LI-COR imager)	LI-COR biosciences	V5.2
CFX Manager 3.1 program	Bio-Rad	N/A
STRING program	https://string-db.org/, Szklarczyk et al., 2017	V10.5
Cluster3.0	bonsai.hgc.jp/~mdehoon/software/cluster/software.htm	N/A
MaxEntScan::score5ss	Yeo and Burge, 2004	N/A
	http://genes.mit.edu/burgelab/maxent/Xmaxentscan_scoreseq.html	
DAVID Gene Ontology	Huang et al., 2009a, 2009b, https://david.ncifcrf.gov	V6.8
Other		
Human genome sequence and annotation (.fasta, .gtf)	UCSC https://ccb.jhu.edu/software/tophat/igenomes.shtml	hg19